Global and Planetary Change 222 (2023) 104057

Contents lists available at ScienceDirect

Global and Planetary Change

journal homepage: www.elsevier.com/locate/gloplacha

Petrological, petrophysical and petrothermal study of a folded sedimentary succession: the Oliana anticline (Southern Pyrenees), outcrop analogue of a geothermal reservoir

Pedro Ramirez-Perez [a,1,*], Irene Cantarero [a], Gabriel Cofrade [a], Daniel Muñoz-López [a], David Cruset [b], Jean-Pierre Sizun [c], Anna Travé [a]

[a] *Grup Consolidat de Recerca Geologia Sedimentària, Departament de Mineralogia, Petrologia i Geologia Aplicada, Facultat de Ciències de la Terra, Universitat de Barcelona (UB), c/ Martí i Franquès s/n, 08028 Barcelona, Spain*

[b] *Group of Dynamics of the Lithosphere, Geosciencies Barcelona (GEO3BCN-CSIC), Lluís Solé i Sabaris s/n, 08028 Barcelona, Spain*

[c] *Chrono-Environnement, UMR CNRS 6249, Université de Franche-Comté, 16 Route de Gray, 25030 Besançon Cedex, France*

ARTICLE INFO

Editor: Liviu Matenco

Keywords:
Geothermal reservoir
Petrophysics
Thermal characterization
Sedimentary petrology
Oliana anticline
Southern Pyrenees

ABSTRACT

The Oliana anticline (Southern Pyrenees) has been characterized as an outcrop analogue of a geothermal reservoir using field data (stratigraphy and fracturing) and petrological, petrophysical and petrothermal analyses. Five lithofacies were established including conglomerates, hybrid arenites, lithic arenites, carbonates and evaporites.

Petrophysical measurements indicate widely dispersed values of bulk density, connected porosity, permeability and velocity of compressional acoustic waves. Connected porosity is the factor that mostly influences bulk density, compressional wave velocity and permeability. In turn, diagenetic processes (such as dissolution and cementation) and fracturing, coupled with petrological features such as mineral composition, matrix content and grain size, are the most critical factors controlling rock porosity along the Oliana anticline.

Thermal conductivity measures reveal a compositional control on the thermal properties of rocks. Thermal characterization of the structure reveals a low conductive area that matches the carbonate and evaporite succession of the anticline core and a highly conductive zone associated with the detrital succession of the fold limbs.

The Oliana anticline has been classified as a petrothermal system due to the low permeability values of the studied sedimentary succession. Despite such classification, this contribution provides a useful exploration tool for future studies of non-conventional geothermal and CO_2 storage sites located in folded sedimentary successions in the proximal domain of foreland basins.

1. Introduction

With increasing global energy demand and the simultaneous need to reduce CO_2 emissions, the current climate and energetic context calls for an increase in natural settings in which CO_2 storage and alternative energy exploitation can be implemented (Tester et al., 2012). In this sense, petrophysical exploration, together with the characterization of the thermal properties of rocks (i.e., thermal conductivity, thermal effusivity and specific heat capacity), can facilitate the discovery of new unconventional geothermal reservoirs. Such reservoirs are here defined as those geological settings that do not exhibit, in the first instance, geothermal anomalies or exceptional permeabilities. Therefore, these geological settings have historically been little studied for geothermal energy production in favour of more conventional regions associated with magmatic activity or the presence of geothermal resources in the subsurface (Huenges, 2010; Moeck, 2014; Breeze, 2019 and references therein). Previous research on rock thermal conductivity showed that this property is positively related to mineral density, whereas porosity is

* Corresponding author.
E-mail addresses: pramirezperez@ub.edu (P. Ramirez-Perez), i_cantarero@ub.edu (I. Cantarero), gcofrade@ub.edu (G. Cofrade), munoz-lopez@ub.edu (D. Muñoz-López), dcruset@geo3bcn.csic.es (D. Cruset), jpsizun@univ-fcomte.fr (J.-P. Sizun), atrave@ub.edu (A. Travé).
[1] postal address: c/ Martí i Franquès s/n. 08028 Barcelona, Spain. Departament de Mineralogia, Petrologia i Geologia Aplicada (Floor 2), Facultat de Ciències de la Terra, Universitat de Barcelona, Barcelona

https://doi.org/10.1016/j.gloplacha.2023.104057
Received 30 May 2022; Received in revised form 1 February 2023; Accepted 2 February 2023
Available online 7 February 2023

typically negatively correlated (i.e., Clark, 1966; Brigaud and Vasseur, 1989; Clauser and Huenges, 1995; Vasseur et al., 1995; Abdulagatova et al., 2009; Fjeldskaar et al., 2009). Fewer studies have established the relationships between rock thermal properties and P-wave velocities (Popov et al., 2003; Mielke et al., 2015). In porous rocks, rock composition, together with pore-space structure, sorting, grain size and cement mineralogy, have been described as the main factors controlling thermal conductivity (Midttømme and Roaldset, 1998; Schön, 2015).

Some of the studies mentioned above focused on improving energy exploitation of conventional geothermal sites associated with thermal anomalies in the subsurface (i.e., shallow hot springs, active volcanic regions, hydrothermal upwellings). However, the most recent studies were carried out to evaluate deeper geothermal reservoirs, including the thermal characterization of the reservoir rocks. In this regard, sufficient temperature (values over 150 °C are already considered suitable for geothermal exploration) and permeability (above 10 mD) have been identified as critical parameters to assess the energetic feasibility of a new geothermal reservoir (Bauer et al., 2017; Kaminskaite et al., 2022; Raymond et al., 2022).

The occurrence of an homogeneous and elevated temperature in a reservoir depends on the heat-transfer mechanism in the reservoir rock (Moeck, 2014; Scheck-Wenderoth et al., 2014). In this sense, conduction is the dominant mechanism in impermeable rocks such as crystalline basements and sedimentary lithologies with low porosity (Moeck, 2014). In contrast, heat is transferred more efficiently by fluid convection in permeable rocks such as porous or fractured successions (Vidal et al., 2016). Thus, knowledge about the petrothermal and petrophysical properties of rocks is key for geothermal exploration. For this reason, research on natural geothermal systems has been focused on studying the geothermal potential of different rock formations by considering their complete set of petrophysical and petrothermal properties (Götz and Lenhardt, 2011; Homuth and Sass, 2014; Aretz et al., 2015; Heap et al., 2017, 2019).

Most of these studies are performed in extensional basins with anomalous geothermal gradients (e.g., the Great Basin, the Molasse Basin, the Upper Rhine Graben, or the Soutz-sous-Forêts geothermal site, Faulds et al., 2011, 2016; Homuth and Sass, 2014; Aretz et al., 2015; Bauer et al., 2015; Homuth et al., 2015b; Heap et al., 2017, 2019). However, advances in geothermal exploration have allowed to establish new potential targets for their geothermal exploitation. In this regard, unconventional geological settings such as Crustal Fault Zones (CFZ) and foreland basins have been proposed as potential sites for producing geothermal energy (Faulds et al., 2016; Hinz et al., 2016; Duwiquet et al., 2020; Sass et al., 2020).

Geophysical surveys applied to geothermal exploration (i.e., 2D and 3D reflection seismics) provide continuous spatial information of relatively large areas (Bauer et al., 2017). This information permits the study of seismic-scale heterogeneities such as permeable fault zones affecting geothermal production. However, due to the resolution of these techniques, the recognition of small-scale structures such as sub-seismic fractures cannot be assessed. In contrast, geophysical and geochemical data acquired from the analysis of core recoveries result in a more accurate and pointed estimation of the properties of a targeted reservoir rock. However, due to the high heterogeneity of sedimentary systems such as fluvial or alluvial successions, well data is not representative of the whole reservoir rock (Müller et al., 2010). In this regard, outcrop analogues allow the characterization of metric to millimetric scale vertical and lateral heterogeneities. Therefore, they represent a solution to appraise the geothermal reservoir potential and understand the limitations of conventional exploration methods (Howell et al., 2014). However, outcrop analogues have not been widely applied for geothermal exploitation and the obtained results are still controversial (Reyer, 2013; Meier et al., 2015). For instance, outcrop data is not always representative of the reservoir properties, as the diagenetic history and pressure and temperature conditions are different between outcropping rocks and their respective buried reservoirs, which represents a significant limitation for geothermal exploration (Beyer et al., 2014; Bauer et al., 2017).

The present study aims to increase the knowledge about unconventional geothermal reservoirs by presenting a combined study of stratigraphic, structural, petrological, petrophysical and petrothermal aspects of the Oliana anticline in the Southern Pyrenees. The excellent outcrops of the Oliana anticline allow us to accurately study the facies composing the different alluvial sequences of the structure and to characterise the stratigraphic and structural features affecting them. Moreover, folded sedimentary successions in proximal domains of foreland basins have been little studied as geothermal reservoirs. Consequently, knowledge about how structure, petrology, petrophysics and petrothermics are correlated in these structures is limited. Specifically, the objectives of this study are threefold: 1) to establish the potential relationships between petrophysical and petrothermal variables, as well as between the structure, stratigraphy and petrological features in the Oliana anticline; 2) to determine the driving factors that explain the variability in the petrophysical and petrothermal properties of the folded sedimentary rocks, and 3) to discuss the feasibility of the Oliana anticline as an outcrop analogue of a geothermal reservoir according to its entire geological characterization.

2. Geological setting

The Pyrenees formed because of the continental collision between the Iberian and the Eurasian plates from Late Cretaceous to Miocene and the subsequent subduction of the former beneath the Eurasian one (Choukroune, 1989; Roure et al., 1989; Vergés et al., 2002; Teixell et al., 2018; Cruset et al., 2020). The collision formed an asymmetric, double verging orogenic belt that resulted from the stacking of thick-skinned basement-involved thrusts forming an antiformal duplex at the center of the chain, named Axial Zone, together with two opposite verging, thin-skinned fold-and-thrust belts (Muñoz, 1992, 2002; Beaumont et al., 2000).

The South Pyrenean fold-and-thrust belt is formed of a piggy-back thrust sequence of south-vergent structures detached above upper Triassic evaporites and lutites (Keuper facies). These evaporites strongly conditioned the location, geometry and evolution of the tectonic structures in the Southern Pyrenees, by forming several diapirs and thrust salients and by transporting the allochthonous units southwards over the Ebro foreland Basin (Vergés et al., 1992; Cámara and Flinch, 2017; Cofrade et al., 2023). The imbricated sequence includes, from north to south and in order of emplacement, the Bóixols thrust sheet, emplaced during the Late Cretaceous (Puigdefàbregas and Souquet, 1986; Saura et al., 2016; Cruset et al., 2020; Muñoz-López et al., 2022), the Montsec thrust sheet, emplaced during the lower Eocene (Mutti et al., 1985), the Serres Marginals thrust sheet emplaced during the upper Eocene (Puigdefàbregas et al., 1986) and the Ebro foreland Basin formed during upper Eocene to Oligocene in the footwall of the South Pyrenean orogenic wedge (Vergés et al., 2002). After the emplacement of the imbricated sequence, the Serres Marginals and Montsec thrusts were reactivated in a break-back sequence from Priabonian to Rupelian (Vergés and Muñoz, 1990; Meigs et al., 1996; Meigs and Burbank, 1997) and were rotated according to a salient, from an original *E*-W orientation to their current NE-SW strike (Sussman et al., 2004). Coevally with this break-back deformation and rotation, the Oliana anticline grew at the footwall of the front of the Serres Marginals and Montsec thrust sheets in the northern margin of the Ebro foreland Basin. It consists of a seismic scale up to 10 km wide and 15 km long fold with a NE-SW orientation (Fig. 1).

Stratigraphy of the Oliana anticline includes upper Eocene to lower Oligocene carbonate, evaporite and detrital *syn*-orogenic strata, comprising limestones, marls, gypsums, sandstones and conglomerates (Fig. 2). The last marine stage of the Ebro foreland Basin was characterized by the sedimentation of the Santa Maria Group (which includes the marls of the Igualada Formation and the limestones of the Tossa

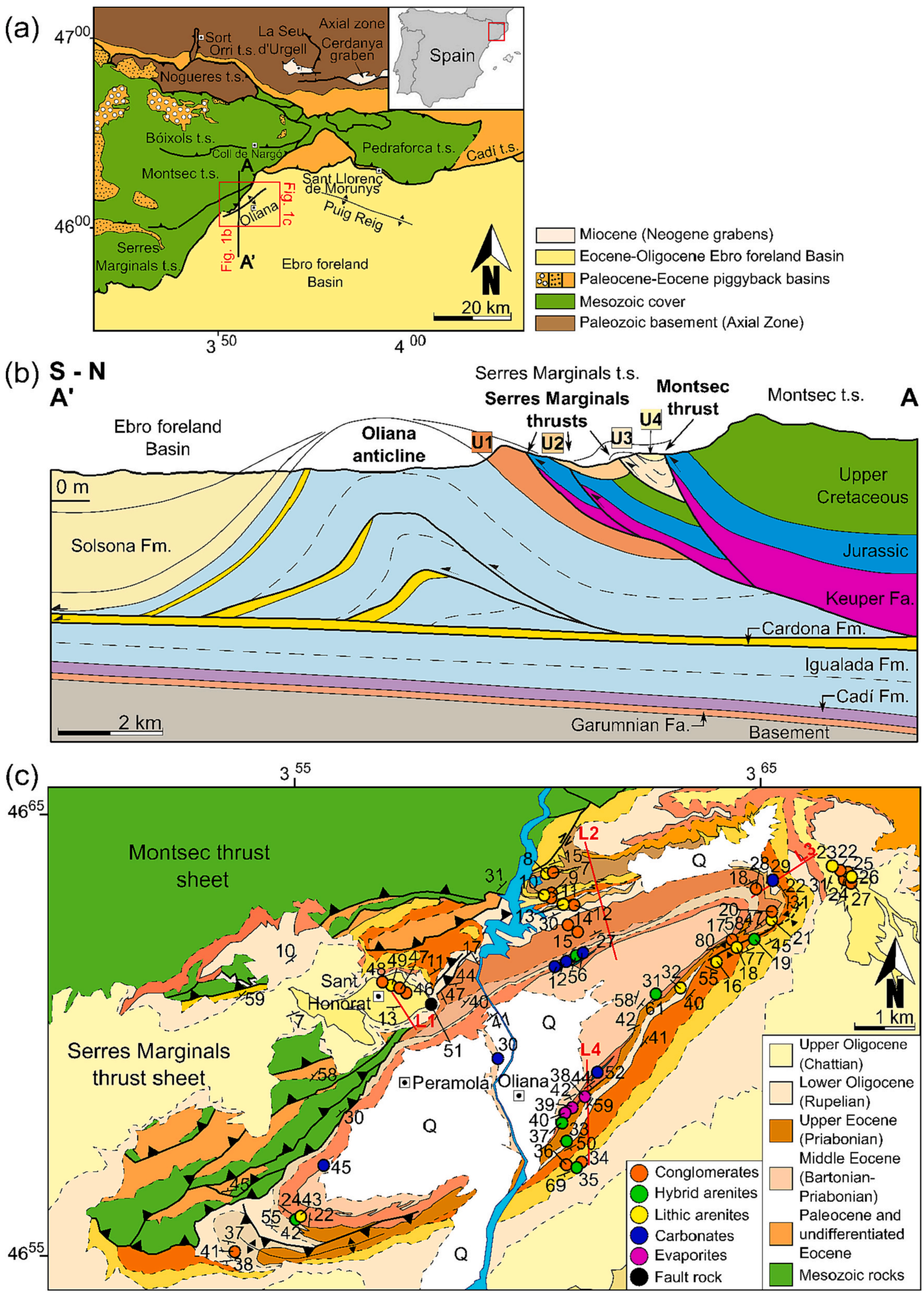

Fig. 1. Geological setting of the Oliana anticline in the Southern Pyrenees. A) Main structural units of Southern Pyrenees showing the location of the Oliana anticline (modified from Vergés, 1993). The A-A' transect and the area inside the red square are shown in figures b and c, respectively. B) S—N cross-section of the South Pyrenean fold-and-thrust belt, including the Oliana anticline (modified from Vergés and Muñoz, 1990). C) Cartography and location of samples of the present study. Dots indicate the position and lithofacies of the samples. Transects L1 to L4 correspond to the stratigraphic logs presented in Fig. 2. Stratigraphic and structural data acquired during fieldwork (i.e., bedding and contacts between units) is included in the cartography. Q refers to Quaternary alluvial deposits. (For interpretation of the references to colour in this figure legend, the reader is referred to the web version of this article.)

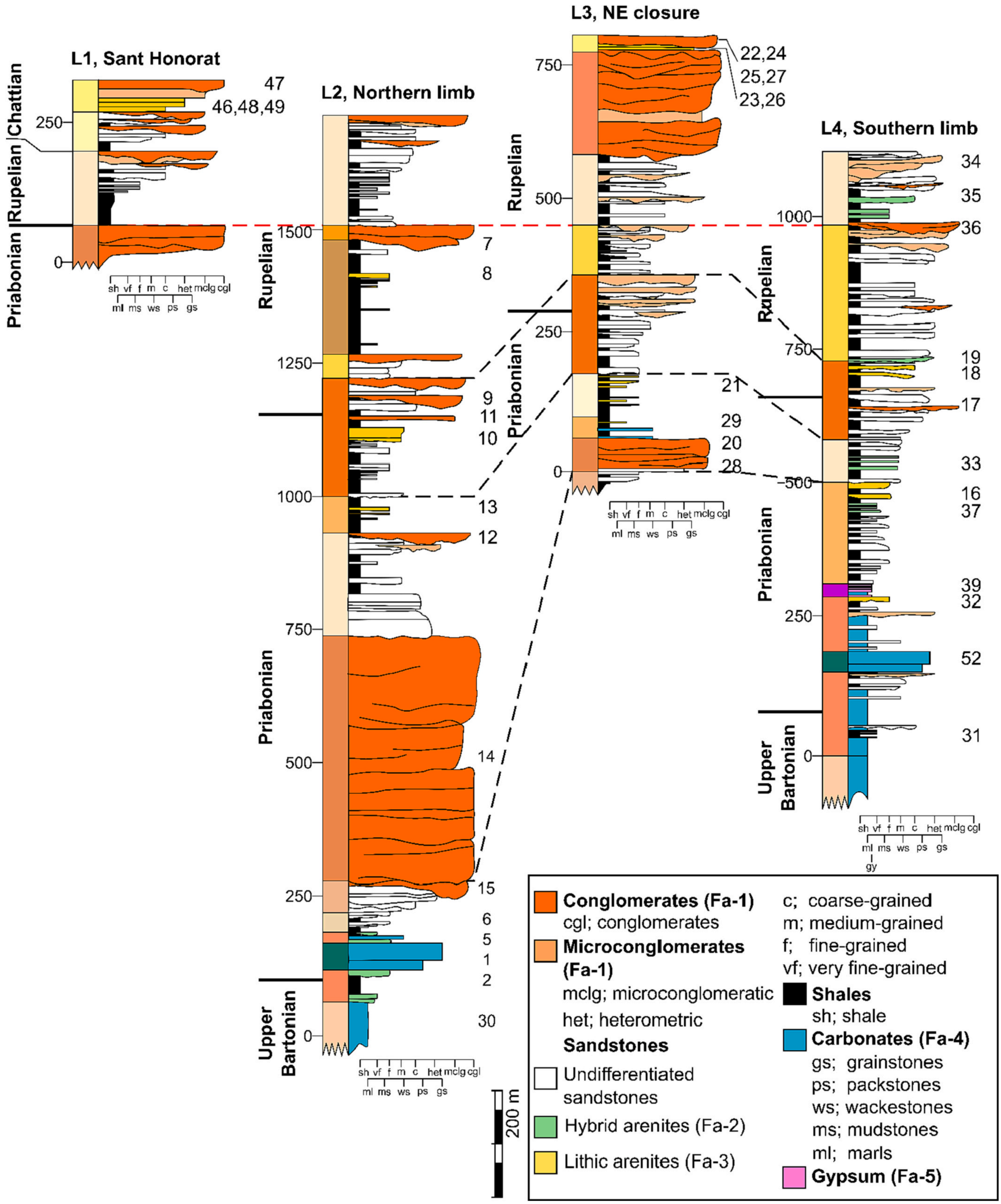

Fig. 2. Stratigraphic logs from Sant Honorat (L1), the northern limb (L2), the NE closure (L3) and the southern limb (L4) of the Oliana anticline, including sample number and sedimentary facies distribution. The location of the logs is referenced in Fig. 1c. The thickness and sedimentology of the unsampled strata are approximative and based on field observations.

Formation) and the overlying limestones of the Terminal Complex (Serra-Kiel et al., 2003a; Cascella and Dinarès-Turell, 2009). Previous studies dated the deposition of these carbonates from the upper Bartonian to the lower Priabonian (Serra-Kiel et al., 2003a). However, more recent palaeomagnetic and biostratigraphic data indicate an age for the marine closure of the Ebro foreland Basin of 36 My, extending the carbonate sedimentation until the middle Priabonian (Costa et al., 2010 and references therein). Accordingly, the deposition of the Cardona Formation evaporites and their marginal equivalent, the gypsums of the Ódena Formation, in an endorheic regime occurred 35 My ago (Costa et al., 2010; Garcés et al., 2020). The detrital succession overlaying these evaporites was formed by different alluvial systems deposited coevally with active tectonics in the Oliana anticline. These alluvial systems are widely associated with the erosion of the allochthonous Mesozoic carbonate rocks during the uplift of the Serres Marginals and Montsec thrust sheets. Although, the uppermost detrital units, Rupelian to Chattian in age, also include igneous and metamorphic lithics, which resulted from the erosion of the Paleozoic basement exhumed in the Pyrenean Axial Zone.

The detrital succession of the Oliana anticline has been sub-divided into four syn-tectonic units, attending to the spatial and crosscutting relationship between the Serres Marginals and Montsec thrust and the conglomerates deposited in front of them in the northern limb of the anticline (Vergés and Muñoz, 1990). These units are bounded by large unconformities originated by the irruption of the different thrusts during the deposition of the syn-orogenic succession. Each conglomerate unit overlaps the previous one and is delimited by a younger thrust to the hinterland following the break-back reactivation (Vergés and Muñoz, 1990).

Based on recent magnetostratigraphic and biostratigraphic data, the following ages have been proposed for these synorogenic units (Costa et al., 2010). Unit 1, cut by the basal thrust of the Serres Marginals, is middle to upper Priabonian. Unit 2, cut by the imbricated Serres Marginals thrust fan, is upper Priabonian to lower Rupelian. Unit 3, cut by the Montsec thrust, is Rupelian in age and Unit 4 is Rupelian to Chattian. The gentle dip angle of the latter unit indicates that thrusting was no longer active in Oliana during its deposition (Burbank et al., 1992; Burbank and Vergés, 1994; Meigs et al., 1996).

3. Materials and methods

3.1. Sampling and structural data acquisition

Fifty-two samples including conglomerates, sandstones, limestones, marls and gypsums were collected along the Oliana anticline and oriented in the field with respect to the bedding strike to compare their petrophysical and petrological attributes parallel and perpendicular to the bedding orientation. Stratigraphic sections were made integrating field data and observations with already published data (the location of samples and logs is displayed in Fig. 1c).

Dip and orientation of fractures and bedding were systematically measured using the FieldMove Clino app and plotted in equal area lower hemisphere Schmidt stereoplots using Stereonet software.

3.2. Petrography

The petrography of sixty-three thin sections was described with an optical Axiophot Zeiss microscope equipped with a Euromex camera. Special attention was paid to the mineralogy and the petrology of the samples, estimating the relative volumetric percentage of siliciclastic versus carbonate components, the occurrence and orientation of fractures and stylolite planes and the description of the porous space geometries to assess the potential pore-connectivity.

3.3. Petrophysics

Sixty-two values (Supplementary material, Table 1) were obtained for measuring the mineral density (ρ_{min}), bulk density (ρ_{bulk}), the compressional velocity of acoustic waves (v_p), connected porosity (N_t) and permeability (K) of 40 samples including conglomerates ($n = 16$), sandstones ($n = 18$), limestones ($n = 5$) and gypsum (n = 1). Samples were sawn into $5.0 \times 5.0 \times 7.0$ cm rock pieces and then drilled into 4.0 $\times$ 5.5 cm cylindrical plugs, which are the maximum dimensions allowed by the Hassler cell and ensure a minimum Representative Elementary Volume (REV) of rock for measuring its properties.

Mineral density and bulk density have been calculated from mass and volume relations following Cavailhes et al. (2013). The volume used for bulk density calculation includes the solid and void volume of rocks that are acquired from water porosimetry. Therefore, the lack of a perfect correlation between bulk density and connected porosity is caused by the different mineralogy (i.e., solid volume) of the plugs. The analytical accuracy for the obtained density values is within ± 0.002 g/cm^3 (Richard and Sizun, 2011).

The compressional velocity of acoustic waves has been calculated in dried plugs using a portable Pundit 6 system (CNS Electronics LTD) operating at a regular frequency of 1 MHz. The absolute uncertainty values for velocity measurements were determined between $\pm$13–96 ms^{-1}.

Connected porosity was measured by water porosimetry using the Archimedes method (Cavailhes et al., 2013), with an absolute accuracy of $\pm 0.05\%$.

Permeability was calculated using a gas permeameter with nitrogen as fluid and the steady-state flow method (Richard and Sizun, 2011; Cavailhes et al., 2013). The pore pressure was controlled using a Hassler cell and data were corrected for Klinkenberg's effect using the graphical method (Riepe et al., 1983; Zinszner and Pellerin, 2007). The relative analytical accuracy is between $\pm 10\%$ (when K $\approx$ 1D) and $\pm$ 0.5% (for K $\approx$ 0.001 mD). The instrumental detection range was 0.001 mD.

3.4. Petrothermics

Fifty-five values (Supplementary material, Table 2) were obtained for measuring the thermal conductivity (τ) and effusivity (ε) of thirty-five samples, including conglomerates ($n = 14$), sandstones (n = 16), limestones ($n = 4$) and gypsum (n = 1). Samples were sawn into slices with a minimum thickness of 3 cm and dried in an oven at 70 °C for at least 24 h. Before measuring, the slices were tempered for 24 $\pm$ 6 h in controlled room conditions (52 $\pm$ 14% of moisture and 22 $\pm$ 3 °C for temperature).

The thermal conductivity and effusivity of rocks have been measured using a TCi thermal analyzer (C-Therm Trident) and the Modified Transient Plane Source (MTPS) method (Di Sipio et al., 2013; Labus and Labus, 2018). Measure accuracy is within 5% of error while the precision of the thermal analyzer equals 1%. The measuring procedure was designed to obtain the most representative petrothermal values of each sample without dismissing their high compositional and textural heterogeneity.

Surfer software has been used to visualize petrophysical and petrothermal data. Gridding was used as the principal interpolation method; consequently, data becomes more artificial far from the measured samples. These data have been represented as "not interpolable" in the figures of this study when they are located further than 50 m from the measuring point. Moreover, due to measuring limitations, a thermal conductivity value of 2.5 Wm^{-1} K^{-1} was assumed for marls (following the data published by Homuth et al., 2011; Homuth et al., 2015a).

4. Fracture characterization

The analysis of the fracture systems in the Oliana anticline has been carried out considering the dip and orientation of the different fracture sets observed along the main structural zones of the fold (i.e., the northern and the southern limbs and the NE and SW closures of the anticline). The chronology of the fractures and the relationships between them were already studied by Sussman (2002) and Sussman et al. (2004).

The occurrence of opened and cemented fractures in the Oliana anticline changes depending on the structural sector of the fold (Fig. 3). In this sense, calcite-filled fractures predominate at the northern limb and the NE closure of the anticline, affecting the detrital succession within Units 1 to 4. In contrast, open fractures dominate at the southern limb and in the SW closure of the fold, affecting Units 1 to 3. In the case of the SW closure, fractures were only measured on rocks of the core of the Oliana anticline and within Unit 1.

Three fracture systems have been described at the northern limb of the Oliana anticline (F1 to F3). Fractures of system F1 have a WSW-ENE strike with a dip angle between 50 and 80° to the north; the F2 system is composed of NNW-SSE striking fractures with a dip angle between 70 and 90° to the east. Finally, fractures within the F3 system display a random strike direction and dip angle between 40 and 60°. F1 and F2 are the predominant fracture systems at the northern limb of the anticline (see Sant Honorat and C-14 Road stereoplots, Fig. 3). Furthermore, the F2 system also occurs in the detrital lithologies in the eastern margin of the southern limb of the anticline. F3 fracture system is common in the Serres Marginals outcropping strata (see Peramola stereoplot, Fig. 3), although the other systems are also present in this sector.

Two more fracture systems have been measured at the southern limb of the anticline (F4 to F5). The F4 system comprises fractures striking W-E and dipping between 45 and 60° to the S-SE, whereas F5 are bed-perpendicular fractures with a random strike direction and dip angle, commonly between 70 and 90°. Overall, F4 is present all along the southern limb, but in its eastern part, the main fracture system is F2 and F5 is rarely present (Fig. 3).

Fracturing at the NE and SW closures of the Oliana anticline is almost perpendicular to bedding with a frequent dip angle between 60 and 90°. The NE closure displays two dominant systems (F6 and F7): F6 strikes NNW-SSE, whereas F7 is *E*-W. The latter system is also observed in the SW closure along with an F8 fracture system, which strikes N-S.

5. Petrology

5.1. Facies description

Five sedimentary facies are distinguished in the Oliana anticline, attending to the composition and texture of the samples: conglomerates (Fa-1, Fig. 4a, b), hybrid arenites (Fa-2, Fig. 4c), lithic arenites (Fa-3, Fig. 4d), carbonates (Fa-4, Fig. 4e) and evaporites (Fa-5, Fig. 4f).

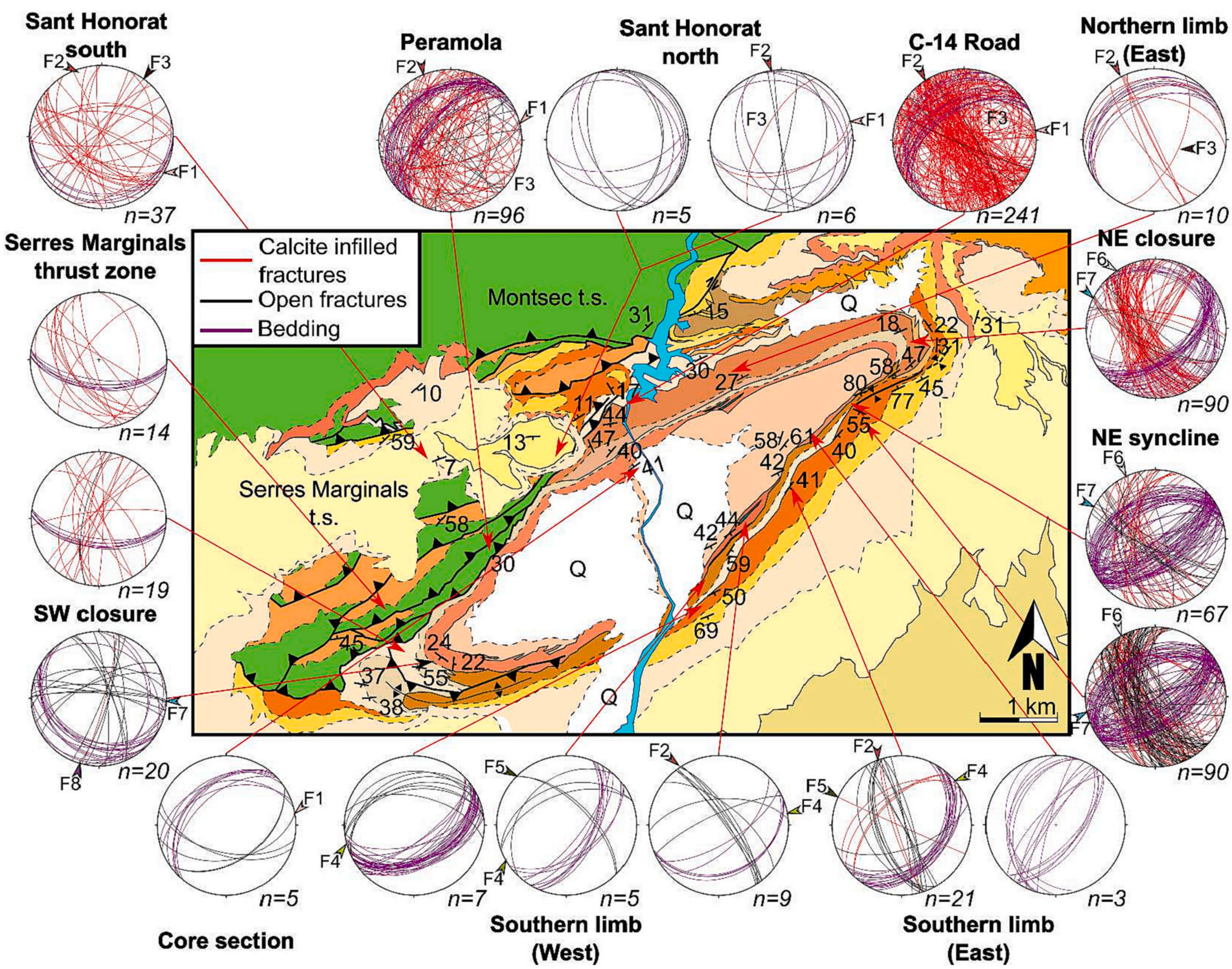

Fig. 3. Lower hemisphere Schmidt stereoplots showing the distribution of fractures through the Oliana anticline according to field observations and measurements, stereoplots of the same fold sector are subdivided according to the tectonosedimentary units in which the fractures were measured. Fracturing is more intense and cemented in the northern limb than at the southern limb and at the NE closure of the fold. The number of measured fractures (n) is given for each stereoplot together with the observable fracture systems (F1 to F8).

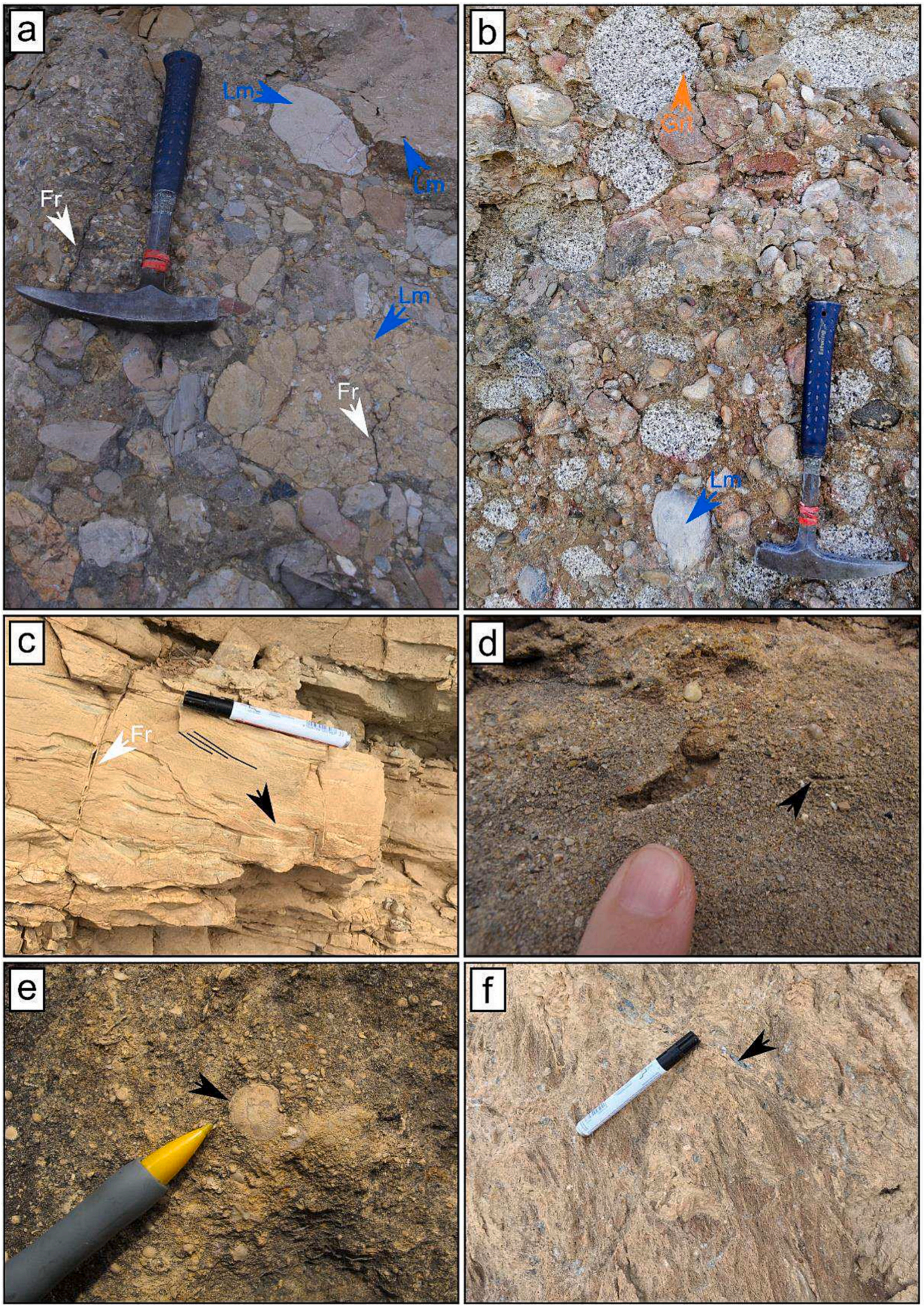

Fig. 4. Field photographs of the studied lithofacies. A) Fa-1, coarse-grained conglomerates of Unit 1 at the northern limb of the fold. B) Fa-1, medium-grained conglomerates of Unit 4 at the northern limb (Sant Honorat region). C) Fa-2, fine-grained hybrid arenite at the southern limb of the anticline. Fractures perpendicular to bedding partially filled by clays and sedimentary structures such as flasher bedding (black arrow) and cross lamination (black lines) are observed. D) Fa-3, fine- to medium-grained lithic arenite at the NE closure. Textural heterogeneity is produced by bioturbation and rip-up clasts (black arrow). E) Fa-4, rudstone from the Terminal Complex at the base of the northern limb of the anticline. Note the abundant fossiliferous content (i.e., Discocycline, black arrow). F) Fa-5, gypsum of the Ódena Fm. at the basal part of the southern limb. Secondary gypsum precipitates in veins (black arrow). Fr, fractures; Lm, undifferentiated limestones; Grt, granite.

5.1.1. *Conglomerates facies (Fa-1)*

This sedimentary facies is represented by clast-supported micro-conglomerates to coarse conglomerates. The coarse fraction contains pebbles from 0.2 to 15 cm, whereas the fine fraction contains grains between 0.05 and 0.2 cm. Components smaller than this constitute the matrix. Conglomerates of Units 1 to 3 are poorer sorted and display more angular quartz grains than conglomerates of Unit 4.

Dolostone and limestone clasts displaying different textures, from mudstones to grainstones, are common in all conglomerate units. The volumetric percentage of carbonate clasts is between 70% and 90% for conglomerates of Units 1 to 3 (Fig. 4a) and between 40% and 60% in Unit 4 (Fig. 4b), and they are smaller in Unit 4 compared to Units 1 to 3. Quartz fragments with anhydrite inclusions (Compostela hyacinth) associated with the upper Triassic Keuper facies are abundant in conglomerates of Units 1 and 2 and are not observed in Unit 4. Similarly, dolostone clasts, arriving from the Jurassic strata cropping out in the Serres Marginals thrust sheet, are more common in Unit 1 than in Units 2 and 3 (Fig. 5a). Metamorphic and granite grains/clasts derived from the erosion of the Pyrenean Axial Zone increase in Unit 4 (Fig. 5b).

Fracture porosity and open stylolite porosity are predominant in conglomerates facies. However, they are reduced by calcite cement precipitation. Compared to coarse-grained ones, an increase in cementation is observed in fine-grained conglomerates and micro-conglomerates. In contrast, fracturing is more abundant in coarse-grained conglomerates than in fine-grained ones.

5.1.2. Hybrid arenites facies (Fa-2)

This sedimentary facies consists of very fine to medium-coarse sandstones (Fig. 4c) with a carbonate content ranging between 50% and 70%. Their grain size ranges between 0.01 and 0.2 cm; sorting is poor to moderate and improves for coarser-grained hybrid arenites. Carbonate components consist of microforaminifers (i.e., Nummulites, incrusting hyaline foraminifera, and other non-identified agglutinated and hyaline foraminifera) and bioclasts (fragments of bivalves, echinoderms, algae and corals). Bioclastic content is higher close to the core of the anticline and decreases progressively away from it (i.e., fine-grained

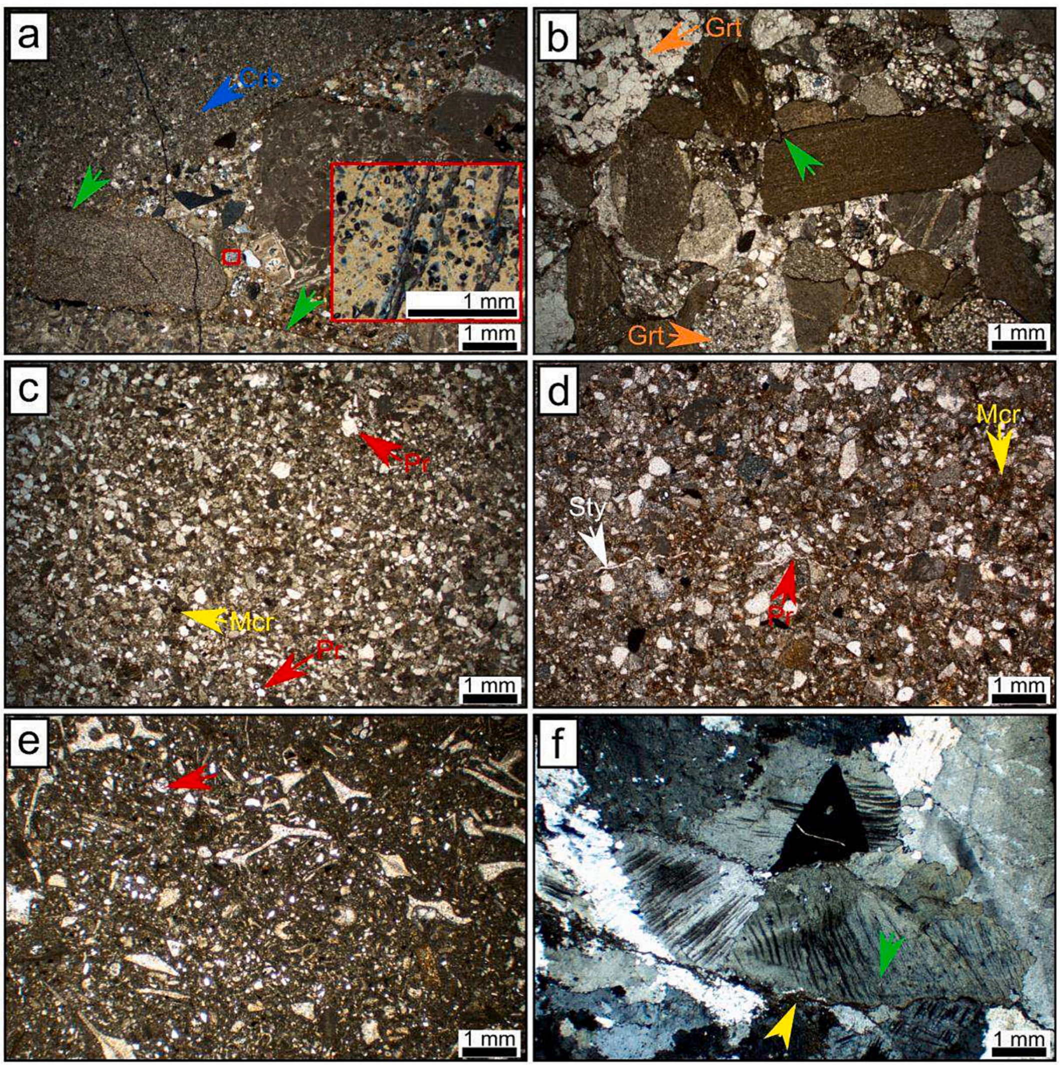

Fig. 5. Photomicrographs of the lithofacies in the Oliana anticline. A) Crossed Nicols. Fa-1, coarse-grained conglomerates from Unit 2 of the northern limb of the fold. The coarse fraction comprises dolomite and limestone pebbles, whereas the fine fraction contains more siliciclastic components. Sutured and stylolitic contacts (green arrows) occur at the contact of pebbles and between the coarse and fine fractions. Reddish accumulations of non-soluble materials fill them. Red square is a detailed image of a Compostela hyacinth derived from the upper Triassic Keuper facies. B) Parallel Nicols. Fa-1, microconglomerate from Unit 4 of the NE closure of the anticline. The coarse fraction comprises more heterogeneous lithics and granite fragments. Although chemical grain contacts predominate (i.e., sutured and stylolitic contacts, green arrow). C) Parallel Nicols. Fa-2, fine-grained hybrid arenite of the southern limb. Vuggy porosity is common in this facies, frequently affecting interparticle calcite cement or punctual micrite accumulations. D) Parallel Nicols. Coarse-grained lithic arenite at the northern limb. The main components are lithic fragments and quartz grains. Open fractures and stylolite planes are also observed. E) Parallel Nicols. Fa-4, packstone of the Terminal Complex of the southern limb. The principal allochems are Discocycline sections, corals and other foraminifers. Moldic porosity is observed. F) Crossed Nicols. Fa-5, Ódena Fm. gypsum at the southern limb. Megacrystalline gypsum crystals contain anhydrite inclusions (green arrow) and frequent accumulations of micrite between their margins. Crb, carbonate pebbles (dolostones and limestones); Grt, granite pebbles; Pr, porosity; Mcr, micrite accumulation; Sty, open stylolites. (For interpretation of the references to colour in this figure legend, the reader is referred to the web version of this article.)

hybrid arenite, Fig. 5c).

Calcite cement is predominant filling the interparticle porosity. Blocky textures and small crystal sizes (up to 0.2 mm) are developed in finner arenites, whereas larger crystals (up to 0.5 mm) in drusy textures are found in the coarser ones. Fe-oxide cement is found in small percentages (1 to 5%) and pyrite often precipitates filling the moldic and intraparticle porosity within bioclasts (1% or less). Bedding parallel lamination and the occurrence of fractures parallel to the micrite laminae are often observed in this facies.

5.1.3. Lithic arenites facies (Fa-3)

This sedimentary facies is constituted of very fine to coarse-grained sandstones with a volumetric percentage of carbonate ranging between 30% and 50%, whereas siliciclastic components represent between 50 and 70%. Grain size ranges between 0.05 and 0.5 cm, slightly coarser, though less sorted than hybrid arenites. The siliciclastic grains of this facies consist of 40–60% of quartz, 10–20% of feldspar, 10–30% of lithic fragments (mainly consisting of Paleozoic phyllites and quartzites, and subordinate Mesozoic dolostones, limestones and quartz with anhydrite inclusions) and 1–5% of muscovite, biotite and minor chlorite. Sorting and roundness are better in fine-grained lithic arenites than in coarser-grained ones (i.e., coarse-grained lithic arenite, Fig. 5d). Two samples within lithic arenites correspond to greywackes because their matrix percentage is higher than 15%.

Calcite cement in lithic arenites displays the same texture and crystal size as in hybrid arenites. Fe-oxide cement is found in a low percentage (5% or less). The occurrence of porosity and fractures is heterogeneous, though an increase of primary interparticle porosity is observed in most lithic arenites compared to hybrid arenites facies.

Lithic arenites have been collected throughout the entire anticline. They are more abundant within Units 2 and 3 at the NE closure and the northern limb of the anticline than in other fold sectors (Fig. 2, logs L2 and L3).

5.1.4. Carbonate facies (Fa-4)

This sedimentary facies is constituted of marls of the Igualada Formation and marls and carbonates from the Tossa Formation and the Terminal Complex (Travé et al., 1996; Serra-Kiel et al., 2003a, 2003b). Grainstones and packstones are composed of Nummulites, algal fragments, corals, bivalves and echinoderms fragments, whereas wackestones contain up to 10% of quartz content.

This facies is highly heterogeneous. Marls and matrix-supported carbonates (mudstones and wackestones) display frequent vuggy porosity, whereas fracture and moldic porosities are predominant in grain-supported carbonates (Fig. 5e). Similarly, the best-cemented carbonates are the grain-supported ones with a cement content between 20 and 25%. In the case of matrix-supported carbonates, Fe-oxides (10 to 15%) and pyrite precipitation (5 to 10%) are more abundant than in grainstones (with a Fe-oxide below 5% and pyrite between 1 and 5%).

Fractures are less common in carbonates than in the detrital facies. They are often cemented in grainstones and partially filled or open in wackestones and packstones. In matrix-supported carbonates, open fractures are frequently developed parallel to bedding, but bed-perpendicular fractures also occur.

Limestones and marls are restricted to the core of the Oliana anticline. In this regard, the marls of the Igualada Formation crop out forming decameter-thick (up to 25 m of thickness) massive bodies, whereas carbonates of the Terminal Complex constitute meter-thick (up to 2 m) strata with restricted lateral continuity as they seem to pinch out into more marly intervals (Fig. 1c).

5.1.5. Evaporite facies (Fa-5)

This sedimentary facies includes gypsum of the Ódena Formation. It occurs at the base of the southern limb in the transition between the carbonates composing the fold core and the detrital succession surrounding them. Evaporites crop out frequently mixed with clays and marls of the underlying Igualada Formation. Gypsum has been classified as secondary megacrystalline with crystals up to 1 mm in size. Anhydrite inclusions and accumulations of micrite at the edge of the crystals are frequent (Fig. 5f).

5.2. Porosity and pore-space connectivity

Primary porosity is principally observed in lithic arenites, whereas secondary porosity is observed in all facies. In this sense, primary porosity is often isolated and poorly connected and pores are often arranged following rock lamination. In the case of secondary porosity, it is produced by different processes such as dissolution (i.e., vuggy porosity, moldic porosity, intraparticle porosity, stylolite porosity) and fracturing (i.e., fracture porosity) that form heterogeneous pore geometries and pore-connectivity. In this sense, even if the description of pore connectivity is limited to a two-dimensional view of the samples, some pore geometries observed in the thin sections are potentially more connected than others and coincide with high permeability values in the respective samples.

Vuggy porosity (μm to mm in size) is commonly developed in carbonate and hybrid arenites facies. This type of porosity develops open spaces without any preferential distribution, though it has also been observed following the lamination of some samples (i.e., fine-grained hybrid arenite, Fig. 6a). In addition, vuggy porosity is higher in areas displaying high micrite content such as bioturbation infills or micrite laminae. Dissolution of the different carbonate components also produced moldic porosity in carbonate and conglomerates facies (by partial dissolution of the carbonate clasts).

Fracture and open stylolite porosity are present in all the facies, being more abundant in the conglomerates, especially, in the coarse-grained ones. Fractures and stylolites are formed surrounding the edge of the pebbles of the coarser fraction, producing a strongly well-connected pore network (Fig. 6b).

5.3. Grain contacts and compaction structures

Punctual grain contacts are abundant in fine-grained lithologies (i.e., fine sandstones), whereas concave-convex and sutured contacts are observed in all samples. Stylolitic contacts are more common in conglomerates, though sandstones also display bed-parallel stylolites.

The average amplitude of stylolites ranges between some μm to mm, being up to centimetric size in the case of coarse conglomerates. Stylolitic planes are preferentially formed parallel to bedding because of burial stresses. However, their orientation is more chaotic in conglomerates, because as stylolites are formed at the margin of the pebbles or following the granulometric contact between coarse components and the fine fraction (i.e., microconglomerate, Fig. 6c).

Moreover, the occurrence of stylolitic planes coinciding with rheological changes (i.e., granulometric changes, bioturbation, or increases of the matrix content) is reported in very fine-grained greywackes (Fig. 6d).

Open stylolites are infrequent as they are commonly filled by non-soluble materials. Moreover, fluid circulation has occurred across some of them because calcite cement is observed filling stylolites. In such cases, regional tectonism is responsible for the opening of stylolites by bed-parallel stresses, which in turn resulted in the formation of bed-perpendicular stylolite planes.

5.4. Cement characterization

Calcite cement is ubiquitous in all samples (Fig. 6). Fine to medium-sized crystals displaying blocky and drusy textures are present in the interparticle porosity. Crystal size increases with pore size and displays drusy and mosaic textures (i.e., microconglomerate, Fig. 6e). Rimmed and bladed calcite are often present in conglomerates (Fig. 6f).

Fe-oxide cement often infills interparticle porosity in sandstones and

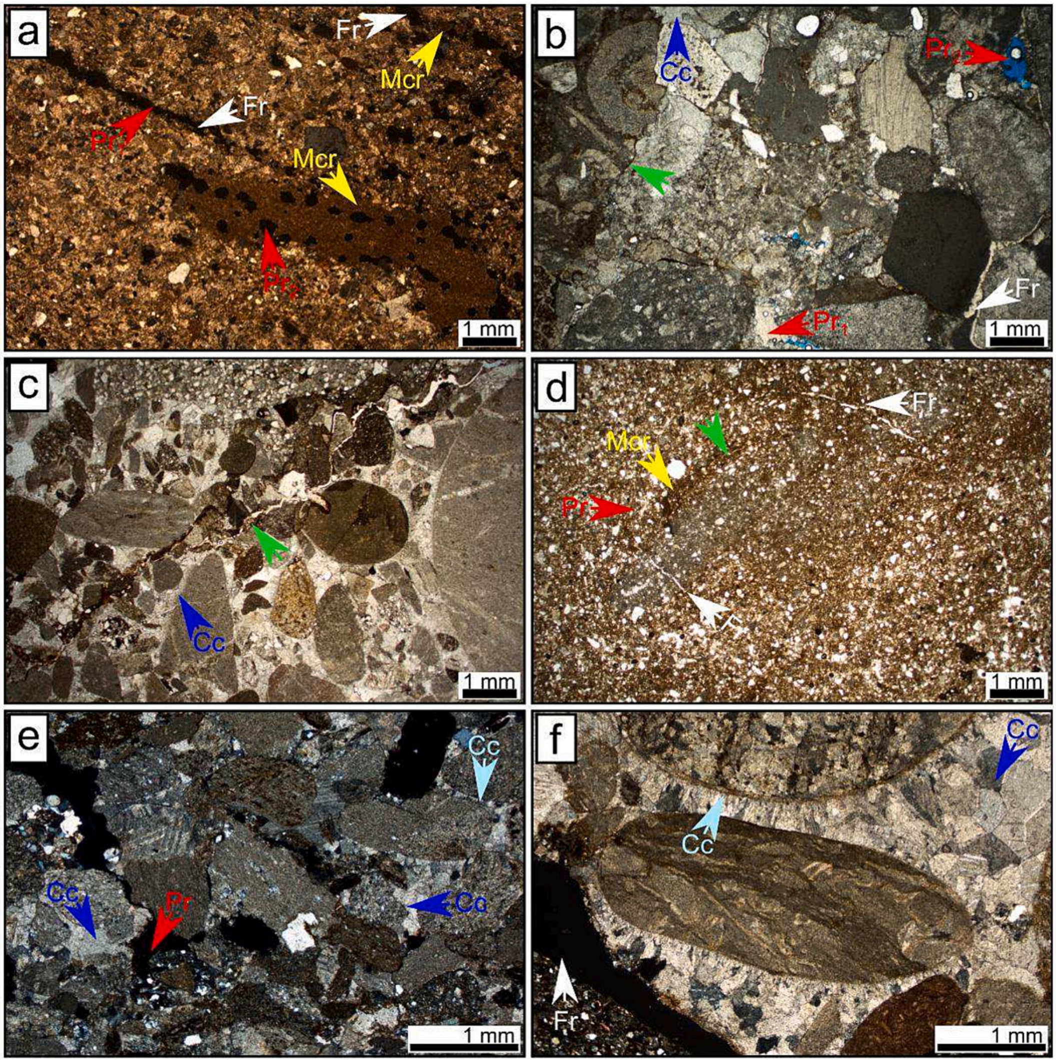

Fig. 6. Porosity, grain contact and cementation microphotographs. A) Crossed Nicols. Medium-grained hybrid arenite from the southern limb of the anticline. Note that open fractures are formed parallel to each other following rock lamination. Fracture and vuggy porosity are observed. B) Parallel Nicols. Coarse-grained conglomerate from Unit 1 of the northern limb of the anticline. Closed stylolite planes are formed at the margin of the clasts (green arrow). Vuggy porosity is formed affecting the calcite cement infilling the fractures and interparticle space. C) Parallel Nicols. Microconglomerate from Unit 4 of the NE closure. An example of a stylolite affecting the fine fraction (green arrow). D) Parallel Nicols. Very fine-grained greywacke from the northern limb of the fold. Open fractures are developed perpendicular to the bioturbation fill whereas stylolite contacts occur surrounding the bioturbation (green arrow). Isolated vuggy porosity is developed in zones with high micrite matrix content. E) Crossed Nicols. Microconglomerate of the northern limb of the fold (Sant Honorat region). Fine to medium-sized drusy (blue arrows) and blocky (light blue arrow) calcite predominates. Note the vuggy porosity (Pr) formed by the dissolution of calcite cement. F) Crossed Nicols. A fine-grained conglomerate of Unit 4 from the NE closure of the anticline. Bladed calcite in rimmed disposition precipitates around grains (light blue arrow). Subsequently, larger calcite (up to 1 mm) precipitates in drusy to mosaic textures (blue arrow). Pr, Porosity; Mcr, Micrite accumulation; Fr, Open fractures; Cc, Calcite cement. (For interpretation of the references to colour in this figure legend, the reader is referred to the web version of this article.)

moldic porosity (i.e., Nummulites) in carbonates. In addition, pyrite has precipitated infilling intraparticle porosity (i.e., chambers of foraminifera) and moldic porosity of hybrid arenites and carbonates. Fracture porosity might be open or total to partially filled with blocky and drusy calcite. Occasionally, dolomitization of the original calcite cement has occurred.

Conglomerates is the most-cemented facies and has the largest crystal sizes (up to 3 mm). In this sense, calcite cement is more abundant in fine-grained conglomerates and microconglomerates (between 20 and 30%) than in coarse-grained ones (usually below 20%). In contrast, the cementation of sandstones and carbonates is variable, with hybrid arenites being the least cemented facies (often below 15%) and having the smallest crystal sizes (below 1 mm).

6. Petrophysical characterization

6.1. Mineral density and bulk density

The mineral density varies from 2.334 to 2.767 g/cm^3, with 91.94% of the measured densities within a range of 2.650 to 2.750 g/cm^3 ($n = 37$ samples, Fig. 7a). This narrow interval coincides with the mineral density values defined by Horai (1971) for calcite (2.72 g /cm^3) and quartz (2.65 g/cm^3) and subordinate dolomite (2.86 g/cm^3) and K-feldspar (between 2.58 and 2.61 g/cm^3). The measured density for the Oliana gypsum is 2.340 g/cm^3, slightly higher than the theoretical value of 2.320 g/cm^3. Usually, mineral density is higher in bed-parallel plugs than in bed-perpendicular ones.

The bulk density in the rocks of the Oliana anticline varies from 2.107 to 2.710 g/cm^3 with 54.84% of the obtained values in a range of

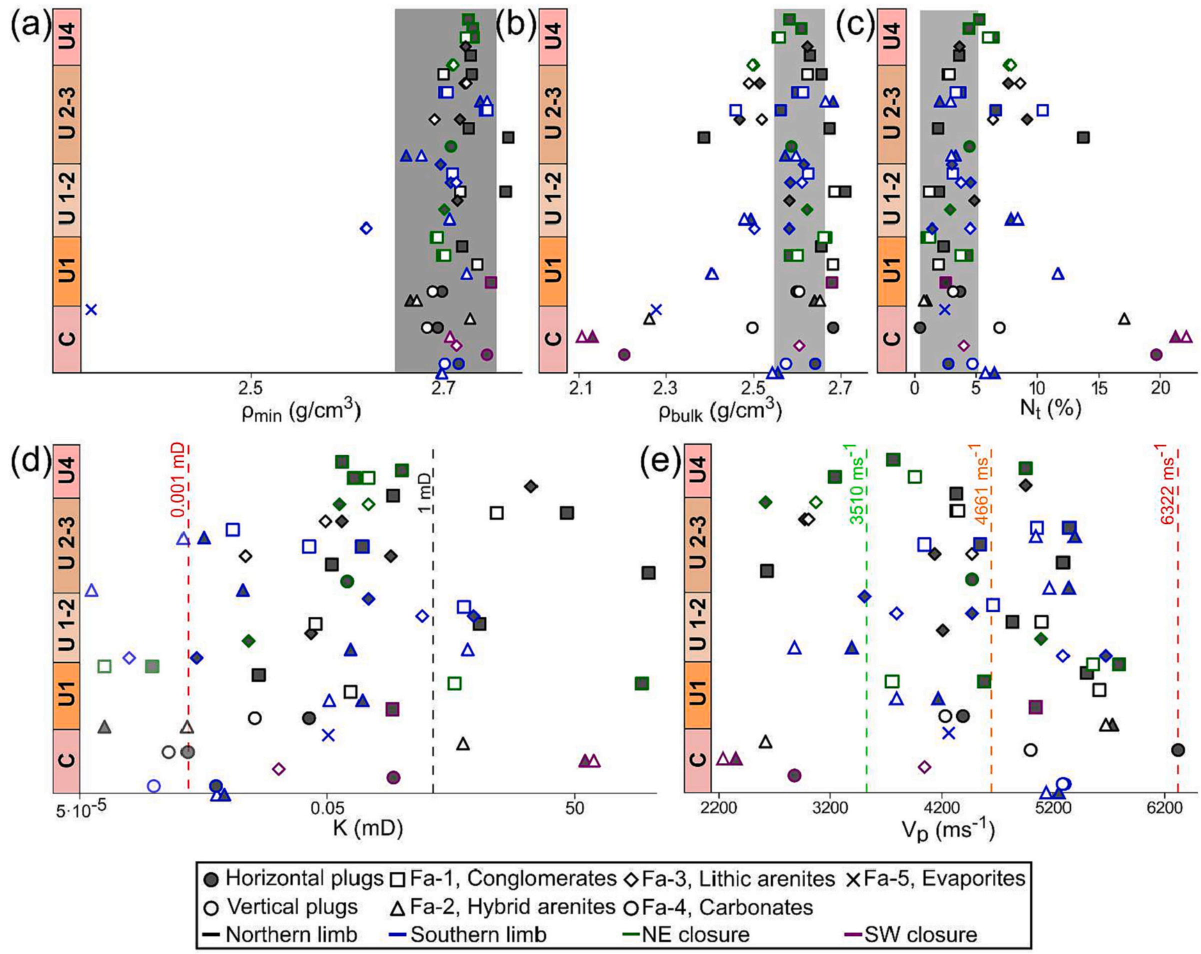

Fig. 7. Petrophysical properties of rocks from the Oliana anticline according to their stratigraphic and structural position. A) Mineral density. B) Bulk density. C) Connected porosity. D) Permeability. E) Velocity of compressional acoustic waves. The vertical axis comprises the stratigraphic units (Core, C, to U4). The shaded area represents the most common range of values for each property. In the case of the last two properties, the considerable dispersion of the values does not allow to provide a representative range and the limits of three intervals are shown. In the permeability graph, the instrumental detection threshold (0.001 mD) is displayed.

2.550 to 2.660 g/cm^3 ($n = 23$ samples, see Fig. 7b). Bulk density shows a higher dispersion than mineral density, though, bed-parallel plugs keep being denser than bed-perpendicular ones.

Conglomerate samples are commonly within the 2.582 to 2.681 g/cm^3 bulk density range ($n = 11$ samples, 65.22% of the measured values), being the densest facies among the studied ones. Carbonates (from 2.573 to 2.641 g/cm^3; n = 3 samples, 62.5% of the values), lithic arenites (from 2.582 to 2.623 g/cm^3; $n = 5$ samples, 53.33% of the values) and hybrid arenites (from 2.405 to 2.596 g/cm^3; $n = 4$ samples, 53.33% of measured values) are comparatively less dense. This section does not consider evaporites due to their partial dissolution during experimental data acquisition.

6.2. Connected porosity

The connected porosity varies from 0.42 to 22.14% in samples of the Oliana anticline, with 64.52% of the values within a range from 0.42 to 5.25% ($n = 28$ samples, Fig. 7c). This property shows a high dispersity of values between the different samples. However, except for lithic arenites, most samples show similar porosity percentages between plugs, being bed-parallel plugs slightly more porous than bed-perpendicular ones.

Conglomerates is the least porous facies with connected porosity in them ranging between 1.90 and 3.73% ($n = 8$, 54.55% of the values). In contrast, the connected porosity of carbonates ranges from 0.42 to almost 20%. The highest values occur in marls and wackestones, while grainstones show low connected porosity. Sandstones show more variable results, with connected porosity varying from 1.41 to 4.87% ($n = 7$ samples, 60% of the values) in the case of lithic arenites and between 0.74 and 4.53% (n = 3 samples, 40% of the values) in hybrid arenites. In turn, hybrid arenites also have the highest value (i.e., 22.42%) among the studied succession.

6.3. Permeability

Matrix permeability ranges from 0.001 to 393 mD. 16.13% of the values ($n = 10$ plugs) are below the instrumental detection range of 0.001 mD; thus, they are rejected for further interpretations. A 62.90% of the values ($n = 39$ plugs) vary from 0.001 to 1 mD. Carbonates are often below 0.05 mD, whereas the remaining facies are usually within the 0.05 and 0.50 mD range. The remaining 20.97% of measures ($n = 13$ plugs) are above 1 mD and only 6.45% of the measurements (n = 4) are greater than 50 mD (Fig. 7d).

High permeabilities are normally associated with conglomerate facies and some lithic arenites. However, there is a substantial dispersion of permeability values between samples and between bed-parallel and bed-perpendicular measurements made for the same sample. Consequently, it is challenging to narrow down the general trends of this property.

6.4. P-wave velocity

Velocities of compressional acoustic waves are classified within three intervals (Fig. 7e). Low velocities vary from 2236 to 3510 ms^{-1}, medium velocities from 3510 to 4661 ms^{-1} and high velocities from 4661 to 6332 ms^{-1}. 20.97% of all the values are low velocities (n = 13 plugs), 35.48% are medium velocities ($n = 22$ plugs) and 43.55% of the values correspond to high velocities ($n = 27$ plugs).

Conglomerates facies and some hybrid arenites are usually associated with high velocities. Medium velocities correspond to hybrid arenites and carbonates facies; however, the velocities of carbonates are considerably variable. The low acoustic velocities cannot be associated with a single sedimentary facies, as samples of all the facies are within this interval.

7. Thermal conductivity of rocks

The thermal conductivity of samples varies from 1.846 to 3.646 Wm^{-1} K^{-1}, with 81.82% of the values within a thermal conductivity range of 2.912 to 3.613 Wm^{-1} K^{-1} ($n = 30$ samples, Fig. 8). The thermal effusivity in the Oliana anticline ranges between 1838.6 and 2753.3 $Ws^{0.5}m^{-2}K^{-1}$. In this sense, values parallel to bedding are more conductive than those perpendicular to it.

Attending to sedimentary facies, thermal conductivity ranges between 3.160 and 3.604 Wm^{-1} K^{-1} for conglomerates; between 3.0 and 3.646 Wm^{-1} K^{-1} for hybrid arenites; between 2.692 and 3.613 Wm^{-1} K^{-1} in the case of lithic arenites, and between 2.465 and 3.232 Wm^{-1} K^{-1} for carbonate facies. In the case of evaporites, a value of 1.846 Wm^{-1} K^{-1} was obtained.

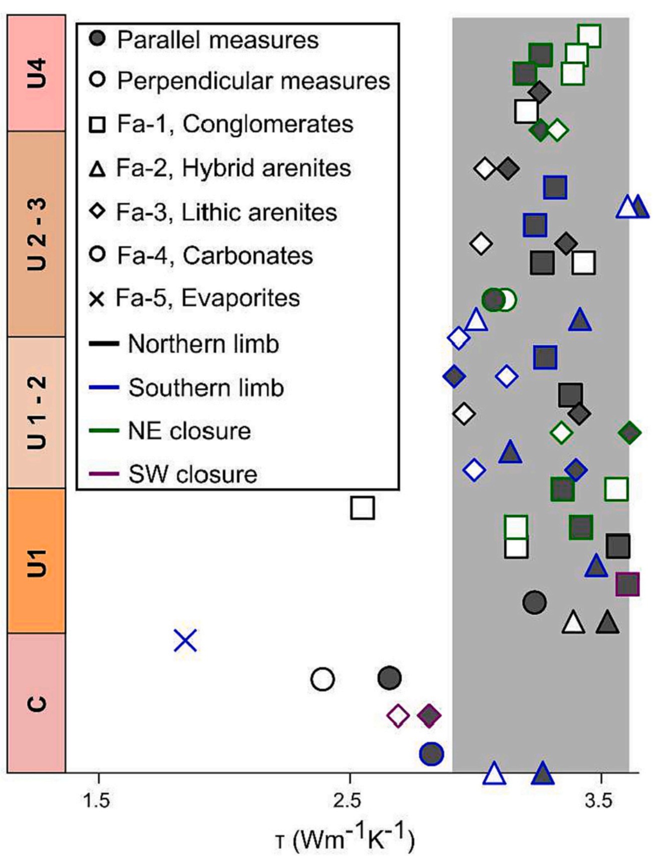

Fig. 8. Thermal conductivity of samples from the Oliana anticline according to their stratigraphic and structural position. The shaded area shows the most common range of thermal conductivity values. The vertical axis comprises the stratigraphic units. Note that the conductivity of the core succession (C) is low compared to the synorogenic sequence (U1 to U4).

Thermal effusivity ranges between 2517.7 and 2734.0 $Ws^{0.5}m^{-2}K^{-1}$ for conglomerates; between 2436.4 and 2753.3 $Ws^{0.5}m^{-2}K^{-1}$ for hybrid arenites; between 2284.0 and 2738.4 W $s^{0.5}$ m^{-2} K^{-1} for lithic arenites and between 2165.3 and 2566.4 $Ws^{0.5}m^{-2}K^{-1}$ for carbonates. The effusivity of the evaporite sample is 1838.6 W $s^{0.5}$ m^{-2} K^{-1}.

The results also show that the values are less variable in conglomerates and carbonates than in sandstones, being the lithic arenites the most heterogeneous facies. The core of the fold, constituted by carbonates, displays lower thermal conductivity values than the detrital synorogenic succession, constituted by conglomerates and sandstones (Fig. 8). Within the detrital succession, the thermal conductivity values of the middle Priabonian and Rupelian synorogenic units (Units 1 and 4, respectively) are comparatively higher and less heterogeneous (varying from 3.160 to 3.604 Wm^{-1} K^{-1}) than the ones acquired from the upper Priabonian and Rupelian synorogenic units (Units 2 and 3, respectively), which have a thermal conductivity range from 2.912 to 3.646 Wm^{-1} K^{-1}, coinciding with more heterogeneous lithologies.

8. Discussion

8.1. Relationship between petrophysics, petrothermics and petrology

This section aims to assess how the petrology of the samples affects the petrophysical and petrothermal properties of the Oliana anticline (data about samples mentioned in this section are found in the Supplementary material). In the case of highly heterogeneous rocks, such as coarse-grained and highly porous ones, a denser sampling was performed during fieldwork to improve the representativeness of the acquired data. Moreover, highly fractured samples were discarded to ensure that petrophysical data reflects the rock properties rather than fracture properties. The comparison between the studied variables establishes that the connected porosity conditions the permeability and compressional velocity of the rocks. Likewise, the thermal conductivity is slightly adjusted to the mineral density of the rocks. The petrological characteristics underlying these relationships are discussed in detail below.

8.1.1. Influence of petrology on pore connectivity

Most of the porosity in the Oliana anticline is formed by open stylolites, open fractures and dissolution of calcite cement, micrite matrix or carbonate clasts. The intensity of these processes (i.e., fracturing and dissolution) explains the differences in porosity through the anticline. For instance, porosity in conglomerates is represented by open fractures and by dissolution of the calcite cement or carbonate clasts.

In the case of the carbonate facies, porosity occurs by dissolution resulting in the formation of vugs affecting the micrite matrix and the calcite cement. Carbonates from the SW closure are more porous (sample PER 45) than those from the NE closure (sample PER 29), the southern limb (sample PER 52) and the northern limb (samples PER 1 and PER 6) of the anticline. Like in conglomerates, changes in the mean porosity of carbonates from different structural zones of the fold may be attributed to the more common occurrence of open fractures, open stylolites and a more intense dissolution in some fold regions (i.e., the SW closure) than in others (i.e., the northern and the southern limbs and the NE closure of the Oliana anticline, see stereoplots in Fig. 3).

The texture of carbonates also plays an essential role in characterizing their connected porosity; higher porosity is measured in samples containing micrite matrix (i.e., wackestones and packstones, PER 45) than in totally cemented ones (i.e., grainstones, PER 1). Besides, bed-parallel open fractures and a more intense dissolution have been observed in the formers, whereas low and isolated vuggy porosity is usually found in the latter.

Primary interparticle and fracture porosity are the main porosity types for lithic arenites. In greywackes (samples PER 8 and 10), dissolution is observed within the matrix, forming isolated vuggy porosity sub-parallel to the sedimentary lamination. The slight dispersion of porosity values acquired in lithic arenites may indicate similar petrological features and dissolution intensity affecting the samples of this facies through the anticline.

The observed porosity in hybrid arenites also occurs as vugs formed by the dissolution of the micrite matrix and the fine to medium-grained interparticle calcite cement. In addition to the matrix content, grain size of the hybrid arenites also affects their connected porosity percentage, as lower values are obtained in coarse-grained ones (i.e., samples PER 5, 19, and 35), than in fine-grained samples (samples PER 2 and 33). This is explained because very fine to fine hybrid arenites are often richer in micrite matrix and contain more fine-grained components that are easier to alter and dissolve (Bell, 1978; Ehrenberg and Walderhaug, 2015; Morad et al., 2018c; Morad et al., 2019). Sample PER 42, with a porosity of 22.42%, is an exception that corroborates the proposal of a more intense dissolution occurring in the SW closure than in the southern and northern limbs of the Oliana anticline.

8.1.2. *Porosity versus permeability*

Although some researchers proposed a direct correlation between connected porosity and matrix permeability (Vernoux et al., 1995; Yang and Aplin, 2010), a clear relationship is not observed in the Oliana anticline (Fig. 9a).

Nevertheless, the permeability measures in Oliana are usually well explained by thin section observations. In this sense, pore geometries potentially connected in this 2D view coincide with high permeability values in the respective samples. In this regard, fracture and open stylolite porosities cause a well-connected pore network, resulting in high permeability values. In contrast, permeability is more heterogeneous and difficult to assess in rocks with dissolution-driven porosity (i.e., vuggy and moldic porosity). Consequently, the modification of the pore space by fracturing, dissolution and cementation also affects the permeability of the rocks within the different facies and fold sectors in the Oliana anticline.

The high permeabilities measured in the northern limb of the anticline (i.e., PER 11, 393 mD) are related to the occurrence of open fractures and stylolites. Moreover, the observed vuggy porosity affecting calcite cement infilling the fractures may indicate some dissolution leading to an increase in the connected pore space. Thus, even if porosity in conglomerates is low, it has strong connectivity explaining the highest permeabilities measured in this facies. These observations also coincide with the higher permeability measured on the bed-parallel plugs coinciding with the preferred direction of stylolites and fractures. The porosity of bed-perpendicular plugs is associated with the margins of the clasts, so it is poorly connected and misoriented.

The lower permeability of the conglomerates at the NE closure of the anticline is explained by the less common occurrence of open stylolites and fractures because of their finer grain size. Moreover, they display a higher degree of cementation, lowering their porosity.

The permeability of sandstones is also strongly influenced by the potential connectivity of the vuggy porosity. In lithic arenites, greywackes display the highest permeability because their higher matrix content allows a greater formation of vuggy porosity. Thus, it is easier to find connected vuggy porosity in greywackes than in other samples of this facies containing less matrix percentage. This fact is well understood if attending to hybrid arenites, which is the facies that display a better positive correlation between connected porosity and permeability (Fig. 9a). Higher permeabilities and connected porosities are measured in fine-grained hybrid arenites than in coarse-grained ones.

Differences in dissolution intensity explain the exceptionally high connected porosity and permeability values of hybrid arenites. In this regard, dissolution features (i.e., vuggy porosity formed by the dissolution of fracture infillings and micrite matrix) are abundant in the SW closure of the anticline. In addition, variation in porosity and permeability within the same structural zone is explained because of the different grain sizes and clay content of the samples. In this sense, coarser grains are demonstrated to be more difficult to dissolve because their specific surface area and reactivity are lower (Bell, 1978; Midttømme and Roaldset, 1998; Ghanizadeh et al., 2015; Carcione et al., 2019).

The permeability and porosity of sandstones in the Oliana anticline increase in bed-parallel direction, often following their lamination. This happens because pores in sandstones are orientated following their

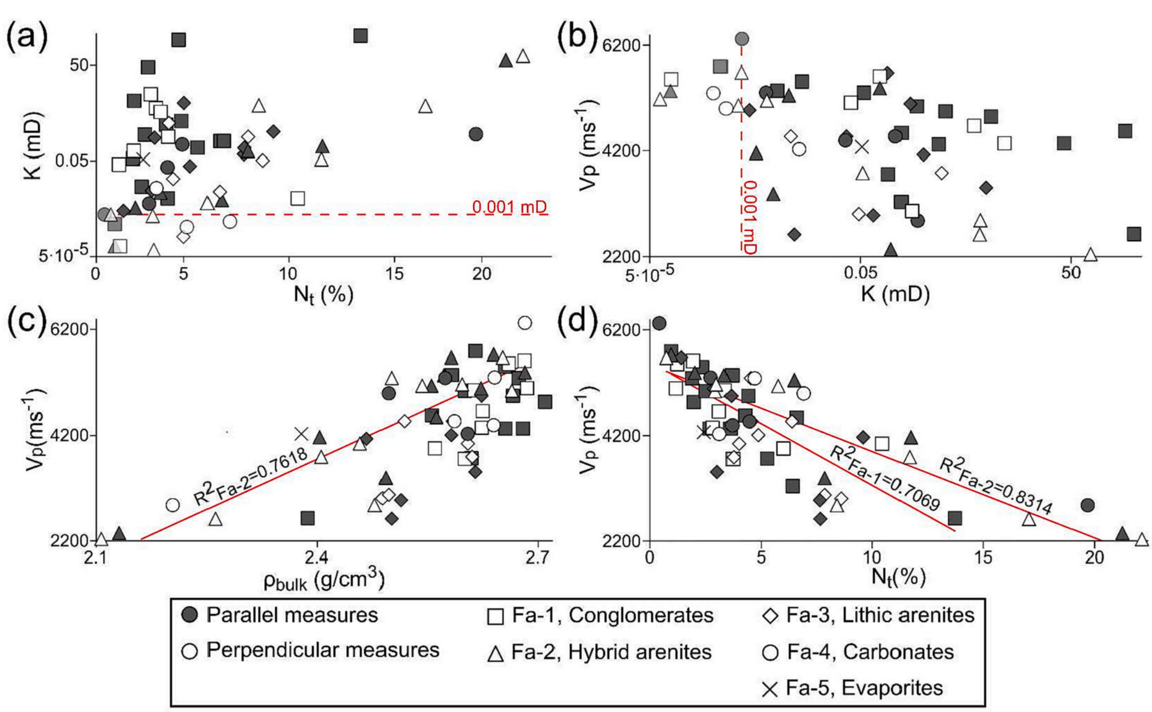

Fig. 9. Relationships between petrophysical measurements in the Oliana anticline. A) Permeability versus connected porosity. The instrumental threshold value is displayed for permeability at 0.001 mD. B) P-wave velocity versus permeability. C) A slight positive correlation between P-wave velocity and bulk density. D) Negative linear correlation between P-wave velocity versus connected porosity.

major axis, which is commonly sub-parallel to bedding (Robion et al., 2014; Farrell and Healy, 2017). Thus, the preferred fracture orientation, the fabric and the dissolution processes should explain the significant permeabilities of the bed-parallel sandstone plugs, as was already reported by Bell and Culshaw (1998) and Farrell et al. (2014) in sandstone formations from England and the North Sea region, respectively.

Regarding carbonates, they show the least permeable values in the Oliana anticline regardless of the structural zone or texture of the sample, meaning that vuggy and moldic porosities in them are poorly connected or intensely filled by calcite cement. In fact, calcite cementation affecting the intergranular pore space in grainstones reduces their potential permeability. At the same time, the abundant microporosity of mud-supported limestones (i.e., mudstones and wackestones) led to technically impermeable values ($K < 10^{-5}$ mD, Bohnsack et al., 2020).

8.1.3. Permeability versus P-wave velocity

A clear correlation is not observed between permeability and P-wave velocity in the Oliana anticline (Fig. 9b). A few studies consider the effect of rock permeability on sonic velocity and there is not a general agreement between authors. However, experimental data demonstrate that compressional waves are transmitted at a slow velocity through fluids (Eberhart-Phillips et al., 1989; Heap et al., 2017). Thus, some authors argue that the acoustic velocity is lowered by open stylolites, open fractures and intensely connected porosity (Mielke et al., 2010, 2015). Consequently, rock permeability and acoustic velocity should be negatively correlated (El Sayed et al., 2015; Al-Dousari et al., 2016). Instead, other authors found that the influence of permeable voids over compressional velocity is neglectable compared to the effect of other petrological features, such as clay content and mineralogy (Heap et al., 2017; Garia et al., 2019, Fig. 9c).

In the Oliana anticline, only conglomerates and hybrid arenites with a connected porosity higher than 3% display a slight negative correlation between acoustic velocity and permeability, coinciding with a negative correlation between the measured connected porosity and acoustic velocity (Fig. 9d). These results agree with the ones presented by other studies on similar rocks (see Garia et al., 2019). Regarding the studied samples, the best-correlated rocks in Oliana are the hybrid and lithic arenites. However, the variability of the measurements does not allow to establish a linear correlation between these variables for sandstones. In contrast, carbonates and greywackes show a poorer correlation, which is in accordance with the study performed by Mielke et al. (2017).

Changes in connected porosity lead to substantial variations in the acoustic velocities of carbonates. This fact agrees with the studies realized by El Sayed et al. (2015) in the Jurassic limestones of Egypt and Heap et al. (2019) in the Muschelkalk formation of Soultz-sous-Fôrets geothermal site in France. The highest velocities measured in the carbonates of the Oliana anticline coincide with the lowest porosities (i.e., sample PER 1, with a 0.42% of connected porosity and a velocity of 6322 ms^{-1} compared to sample PER 45, 19.69% and 2880 ms^{-1}).

Porosity also explains the unusual low acoustic velocities of some conglomerates. Even if the values of this facies are generally well clustered, the compressive acoustic waves show lower velocities with increasing porosity (i.e., sample PER 11, with a 13.72% of connected porosity and a velocity of 2632 ms^{-1}). In fact, grain size, gravel content, cementation type and porosity have been demonstrated to affect the P-wave velocity of conglomerate rocks (Hang et al., 2022). Although none of these relationships is clearly observed in Oliana, they may explain the scatter observed in the data for conglomerate facies (Fig. 9c,d).Samples have been widely collected through the anticline to improve the sampling representativeness of this highly heterogeneous facies, but conglomerates still display different P-wave velocities probably because of the effect of gravel content and grain size (that varies from <1 cm of diameter to 4 cm in the measured plugs), as all of them display calcite cement and a poor correlation between porosity and P-wave velocity (Fig. 9d).

Consequently, the measured values of permeability and acoustic velocity in the carbonates and sandstones of the Oliana anticline are strictly related to rock porosity and the diagenetic processes that modify it, either to increase it (fracturing and dissolution) or decrease it (cementation). In the case of conglomerates, other textural and compositional aspects such as gravel content and grain size may also affect P-wave velocity.

8.1.4. Thermal properties versus petrophysics

Thermal conductivity values show a slight positive correlation with mineral density (Fig. 10a). In contrast to previous studies (Clauser and Huenges, 1995; Mckenna et al., 1996; Abdulagatova et al., 2009; Mielke et al., 2017), the measurements in the Oliana anticline do not show changes in thermal conductivity when changing connected porosity (Fig. 10b), permeability (Fig. 10c) and compressional acoustic velocity (Fig. 10d). Although thermal conductivity values are significantly clustered, conglomerates and hybrid arenites are more conductive than lithic arenites and carbonates in the Oliana anticline.

Previous researchers extensively studied the control of mineral density on thermal conductivity (Clark, 1966; Brigaud and Vasseur, 1989). Their results showed that the petrothermal properties of sedimentary rocks are determined by the thermal properties of their main mineral components. Therefore, the mineral density and thermal conductivity of sedimentary rocks are given by their composition (Clauser and Huenges, 1995). Furthermore, detrital rocks are often more conductive than carbonate rocks (Luo et al., 1994; Heap et al., 2019).

In this regard and according to the data published by Birch and Clark (1940), Horai (1971), Sass et al. (1984) and Čermák and Rybach (1989), from the principal mineral constituents of the rocks studied in Oliana, quartz is the most conductive one (its values vary from 7.0 to 7.7 $Wm^{-1} K^{-1}$), whereas calcite (from 3.26 to 3.60 $Wm^{-1} K^{-1}$), feldspar (from 2.3 to 3.0 $Wm^{-1} K^{-1}$) and dolomite (from 4.6 to 5.5 $Wm^{-1} K^{-1}$) are less conductive.

Attending to the results of the Oliana anticline, a compositional and petrological control on the thermal properties of the rocks is demonstrated since detrital rocks such as conglomerates and arenites (including quartz and dolostone as well as carbonate clasts and grains) tend to be more conductive than carbonates (the average thermal conductivity of the detrital succession in the Oliana anticline is 3.226 $Wm^{-1} K^{-1}$, whereas the average value for the carbonate succession is 2.893 $Wm^{-1} K^{-1}$, see Figs. 8 and 10).

The compositional similarity of the detrital facies explains the subtle variation of thermal conductivity between them. However, although the sediments forming the detrital rocks in the Oliana anticline are derived from the erosion of the same structural units (i.e., the Serres Marginals and Montsec thrust sheets and the Axial Pyrenees), different thermal conductivity and compositions exist between rocks of the same lithofacies that belong to different tectonosedimentary units. For example, conglomerates of Unit 1 (thermal conductivity varies from 3.160 to 3.604 $Wm^{-1} K^{-1}$) are more conductive than those of Units 2 and 3 (between 2.912 and 3.646 $Wm^{-1} K^{-1}$) and Unit 4 (3.201 to 3.450 $Wm^{-1} K^{-1}$).

The observed change of thermal conductivity along the stratigraphic units should be associated with the mineral composition of these rocks because 1) the mineral density of rocks also varies slightly, and 2) for the same structural zone, the grain size of the conglomerates remains similar across the different units. Therefore, grain size does not influence their conductivity.

Based on the petrological analysis, the conglomerates of Unit 1 are richer in carbonate clasts (around 60%) than those of Unit 4 (40%). However, the Unit 1 conglomerates show abundant dolomite clasts and Compostela hyacinth grains, which must account for their higher mineral density (Fig. 7a) and thermal conductivity (Fig. 8). These components are associated with the erosion of the upper Triassic Keuper facies and Jurassic succession that outcrop associated with the detachment level of the Serres Marginals thrust sheet.

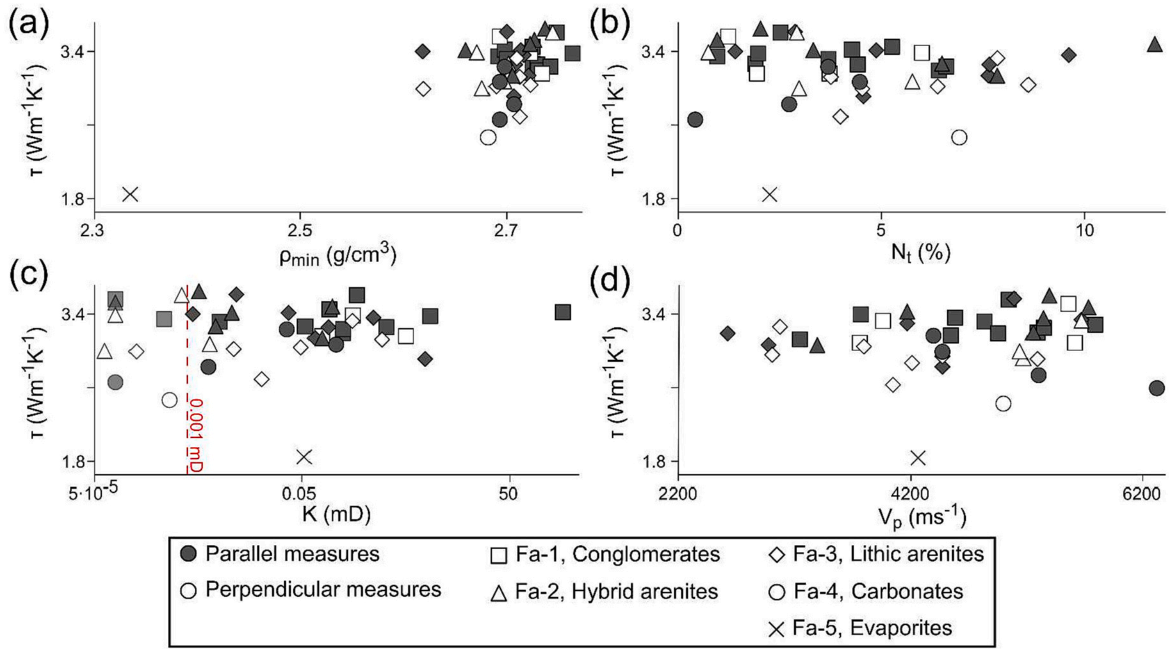

Fig. 10. Thermal conductivity. A) A slight positive correlation is observed between thermal conductivity and mineral density. B) Thermal conductivity versus connected porosity. C) Thermal conductivity versus permeability. D) Thermal conductivity versus acoustic velocity.

The overlaying conglomerate units show a progressive decrease of Keuper quartz grains (they represent 10% of grains in Unit 1 conglomerates and less than 1% in conglomerates of Unit 3) and Jurassic dolostone clasts (they represent almost 30% in Unit 1 conglomerates, whereas the volumetric percentage of dolostone clasts in conglomerates of Unit 3 and 4 has been estimated between 5 and 10%). Although dolostone clasts are found until Unit 4, Triassic quartz grains have not been observed within this last conglomerate unit in the Oliana anticline. At the same time, calcareous clasts associated with the erosion of the Early and Late Cretaceous succession that crop out in the upper parts of the Serres Marginals and Montsec thrust sheets are more abundant in the case of Units 2 and 3 conglomerates. The increase in the thermal conductivity of Unit 4 conglomerates is explained by the higher content of igneous lithics (i.e., granite) and quartz in them, eroded from the Axial Pyrenees.

In the case of sandstones, clay minerals of the matrix act as isolating components that reduce the thermal conductivity of these rocks (Vasseur et al., 1995). However, the most remarkable variation of thermal conductivity in the Oliana arenites coincides, as in the conglomerates, with their stratigraphic position (Fig. 8). Agreeing with previous researchers, the slight thermal variability between sandstones of the same stratigraphic unit is explained by the effect of grain size and matrix content that reduce the effect of mineralogy on the thermal properties of sandstones (Midttømme and Roaldset, 1998).

For example, the higher matrix content of the greywackes of Units 2 and 3 (samples PER 8 and 10) drives to a lower conductivity of them if compared to the hybrid arenites of the same unit (sample PER 35, Supplementary material, Table 2). In addition, the higher thermal conductivity of hybrid arenites than lithic arenites of Units 1 and 2 is explained by the coarser grain size of the formers. For the remaining units, lithic arenites facies is more conductive than hybrid arenites due to their more detrital composition. Sandstones from the core unit are the least conductive rocks, coinciding with a higher carbonate content (Figs. 8 and 10).

As for petrophysics, a texture-specific trend is observed regarding the thermal conductivity of carbonates. Remarkably, the values measured on grainstones and packstones (i.e., samples PER 1 and 52) are lower than the conductivity value of calcite (3.26 ± 0.23 $Wm^{-1} K^{-1}$, according to Brigaud and Vasseur, 1989) probably because of the effect of open fractures in them. In contrast, wackestones (i.e., samples PER 6 and 29) show values closer to the conductivity of calcite (thermal conductivity measured in wackestones varies from 3.06 to 3.232 $Wm^{-1} K^{-1}$). In this sense, the studied wackestones have a certain quartz content (between 5 and 10%) that may increase their thermal conductivity, overcoming any insulating effect of the micrite matrix nor porosity.

8.2. *Control on petrological, petrophysical, and petrothermal parameters in the Oliana anticline*

Fig. 11 displays the petrophysical properties of the different fold sectors of the Oliana anticline and evidences a correlation between the most common facies of a structural zone and its petrophysical characteristics. Consequently, the petrophysical properties in the Oliana fold can be established by attending to the petrological features of the different lithofacies (Fig. 12). However, the influence of the tectonic evolution and the structure on petrology and petrophysics must also be considered.

Thrusting during the upper Eocene produced an active tectonic zone in the NW of the anticline and a passive area in the south. This activity controlled the arrangement of the different alluvial fans in the Oliana fold (Burbank and Vergés, 1994; Sussman and Curtin, 2002). For instance, the most proximal facies predominate to the north, associated with the filling of paleovalleys formed by flexure at the front of the Serres Marginals and the Montsec thrust sheets (i.e., the conglomerates of Units 1 to 3, Fig. 2 logs L1 and L2). The facies gradually become more distal towards the south (i.e., hybrid and lithic arenites of Units 1 to 3, Fig. 2 logs L3 and L4). Therefore, the distribution of the Priabonian to Rupelian synorogenic facies was directly controlled by the coeval thrusting in the NW sector of the studied zone.

Thrusting was no longer active during the deposition of the conglomerates of Unit 4 (Vergés and Muñoz, 1990). Therefore, the distribution of the alluvial fans at this time was initially controlled by the inherited relief and the distance from the Axial Pyrenees. In this sense, the most proximal deposits of the alluvial fans of Unit 4 are located north of the Oliana anticline, whereas the most distal sedimentation was recorded to the south, towards the Ebro foreland Basin (Sussman and

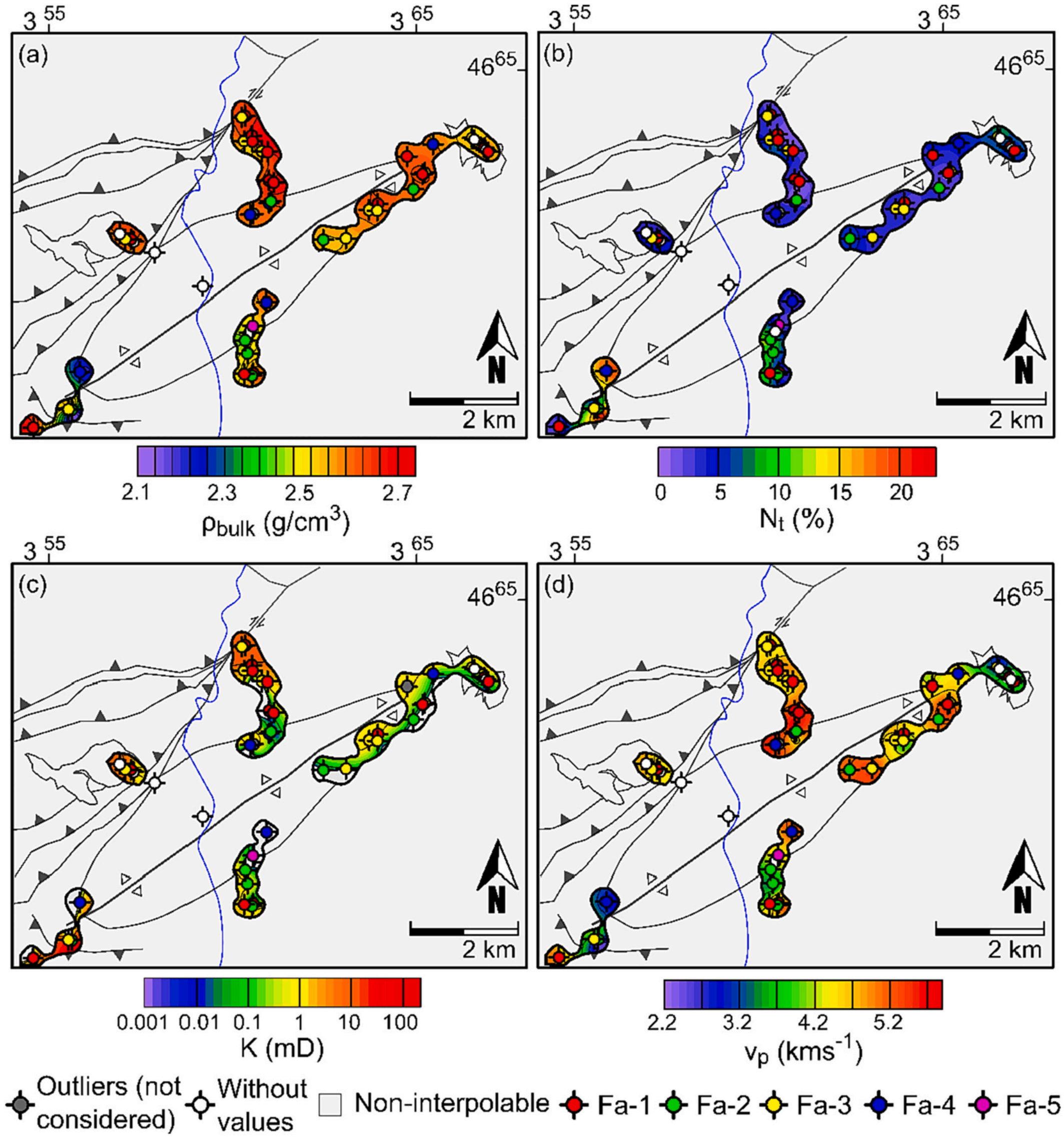

Fig. 11. Mapping of the petrophysical properties measured in the Oliana anticline. A) Bulk density. B) Connected porosity. C) Permeability. D) P-wave velocity. The abnormal values (outliers) detected in Fig. 7 have not been considered at the time to develop the data interpolation in Surfer. The position of the samples is the same as in Fig. 1. The most important structural features of the Oliana anticline are also displayed (e.g., the U4 conglomerate bodies of the NE closure and the northern limb of the fold, the Serres Marginals and Montsec thrusts and the trace of the Oliana anticline).

Curtin, 2002). The fine-grained conglomerates and microconglomerates abundant in the NE closure of the anticline must indicate an intermediate zone between the proximal and the distal deposits of these alluvial fans.

Diagenetic processes commonly modify the petrophysical characteristics of sedimentary rocks (Beyer et al., 2014). For instance, compaction and cementation significantly reduce the effective porosity and permeability of sedimentary rocks (Houseknecht, 1987, 1988; Aretz et al., 2015). In the Oliana anticline, fracturing, dissolution and cementation are the main processes affecting the petrophysical properties by producing or occluding secondary porosity and by altering the original characteristics of the studied rocks, as has been reported in sandstones from reservoirs all over the world (Bjørlykke et al., 1989; Worden et al., 1997; Iyare et al., 2020). Moreover, the petrophysical and petrological study of the Oliana samples suggests that rock porosity is the main factor explaining the variability observed in the other petrophysical properties.

For instance, higher porosity in particular sectors of the Oliana anticline is explained by the different intensities of fracturing, dissolution and cementation. More intense fracturing occurs in the northern limb and the NE closure than in the southern limb of the fold. However, fractures in the northern limb are usually filled with calcite, whereas they remain open at the southern limb of the anticline (see Fig. 3). Two main hypotheses should explain the differential precipitation of calcite cement along the anticline: 1) the occurrence of more intense dissolution at the southern limb than in the rest of the anticline, and 2) a higher degree of cementation in the fractures of the northern limb, as well as in the rocks of the NE closure of the fold, caused by a more intense migration of fluids expelled from the internal part of the Southern Pyrenees and transported following the pathways of the Serres Marginals and Montsec thrust planes (as proposed by Oliver, 1986 and then studied by Bitzer et al., 1998; Lacroix et al., 2014; Cruset et al., 2016, 2018; Nardini et al., 2019; Muñoz-López et al., 2020a, 2020b, Muñoz-López et al., 2022; Sun et al., 2022 in the Southern Pyrenees). Thus, cementation is more intense closer to the orogenic thrusts.

The second hypothesis would also explain the abundance of fractures in the north caused by the tectonic stress of these thrusts. Consequently, the regional tectonic activity should explain the differential diagenetic

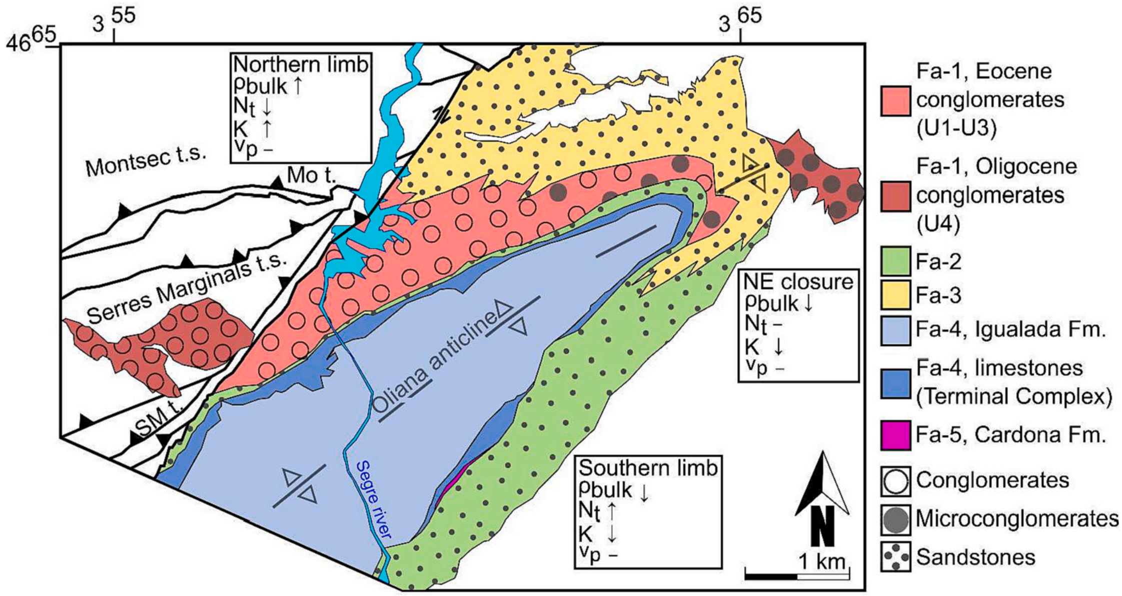

Fig. 12. Summary of the petrophysical properties in the Oliana anticline. According to the results shown in Fig. 7 and Fig. 11, the northern limb is the densest and most permeable zone of the structure, with a clear predominance of the conglomerate facies. To the NE closure, the facies are more distal. Lithic arenites and microconglomerates of Unit 4 are present in this area. Generally, the properties of this zone are intermediate between the ones observed for the northern and the southern limbs. Finally, the southern limb shows the most distal sedimentary facies (coinciding with Sussman and Curtin, 2002) with an increase of the carbonate content. Hybrid arenites are the predominant facies leading to more connected porosity and a decrease in the bulk density of the rocks. However, the permeability in this zone is low. The core of the anticline has not been characterized because of the few samples and the technical problems when processing them. t = thrust; t.s. = thrust sheet; SM = Serres Marginals; Mo=Montsec.

features observed in the Oliana anticline and the petrophysical values produced by modifying the primary porosity of the rocks.

8.3. Contribution of the study to the geothermal research

The thermal conductivity data obtained in the Oliana anticline agree with previous studies for rocks of similar composition and granulometry (Fuchs et al., 2013; Homuth et al., 2015b; Haffen et al., 2017). The petrothermal characterization of the Oliana anticline distinguishes two main lithological groups: 1) the carbonates (marls and limestones) that crop out in the core of the anticline with low thermal conductivities, and 2) the more conductive detrital succession (sandstones and conglomerates) located at the outermost part of the fold. Evaporites are the least conductive rocks (Supplementary material, Table 2).

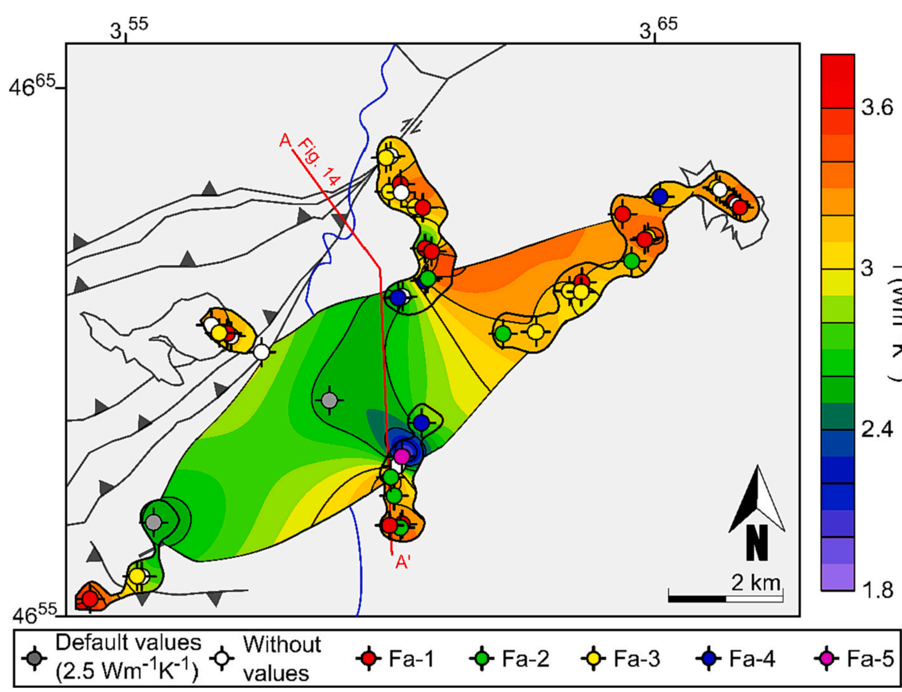

Fig. 13. Mapping of the thermal conductivity in the Oliana anticline. A low conductive zone is observed in the core of the anticline, coinciding with marls, carbonates and evaporites. In comparison, the detrital succession that predominates at the northern limb and the NE closure shows greater conductivities. The gray zone represents an area without measurements. The position of the samples is the same as in Fig. 1.

The petrophysical variation of the lithofacies across the Oliana anticline must be attributed to different processes linked to the tectonic, burial and diagenesis history of the rocks composing this fold, modifying their primary porosity (fracturing, dissolution and cementation). However, variation of the petrothermal properties through the Oliana structure coincides with changes in the general composition of the rocks being the highest conductivities within the detrital succession (Fig. 13). Thus, it can be established that there is an accurate compositional control on the thermal properties of these rocks. In this sense, sandstones and conglomerates are compositionally more heterogeneous than marls, limestones and gypsums, leading to higher conductivities. Therefore, the thermal conductivity of a given area in the Oliana anticline is directly correlated to the composition of the lithology found there, independently of any other petrophysical or diagenetic characteristics.

Permeability is one of the most critical parameters to assess a potential geothermal reservoir. The values obtained in the Oliana anticline are lower than those reported by previous studies for similar settings (Mielke et al., 2010, 2017; Kushnir et al., 2018; Garia et al., 2019). Thus, the Oliana sedimentary succession ranges from impermeable (in the magnitude of 0.001 mD or 10^{-18} m^2) to slightly permeable (393 mD, in the order of 10^{-13} m^2) values. The average permeability of the samples is within a magnitude of 10^{-15} m^2 (1 mD), one order of magnitude below the threshold permeability value typically used in geothermal exploration to evaluate a reservoir as feasible (above 10 mD, Kaminskaite et al., 2022; Raymond et al., 2022).

Based on the obtained matrix permeability results, the sedimentary succession in the Oliana anticline should be classified as a petrothermal system from the characterization of geothermal reservoirs proposed by Sass and Götz (2012). In the studies by Sass and Götz (2010, 2012), alluvial successions are classified as hydrothermal systems due to the high conductivity and permeability of the alluvial facies. However, the low permeability measured in the rocks from the Oliana anticline would hinder the convective movement of hydrothermal waters and their associated heat preventing the main heat-transfer mechanisms of hydrothermal geothermal systems (Huenges, 2010; Moeck, 2014).

Nevertheless, the characterization of fractures and stylolites is essential in studying possible geothermal reservoirs as they would improve or worsen the reservoir quality by modifying its permeability and fluid circulation pathways or by causing hydrothermal alteration of the rocks (Laronne Ben-Itzhak et al., 2014; Martín-Martín et al., 2018; Morad et al., 2018b; Watkins et al., 2018; Humphrey et al., 2019; Chabani et al., 2021; Gomez-Rivas et al., 2022; Sun et al., 2021a, 2021b). For instance, closed stylolites significantly reduce the permeability of the reservoir rocks. Previous research reported the differential formation of stylolites across anticlines, concluding that stylolitization is much more common in the limbs of anticlines than in the crest of the folds (Ehrenberg et al., 2016; Paganoni et al., 2016; Morad et al., 2018a). In the case of the Oliana anticline, the crest of the fold has been eroded, so the study of fractures and stylolites is restricted to the limbs and closures of the fold. We found that in these sectors of the Oliana anticline, the stylolites and fractures occur more frequently in detrital facies than in carbonate units, showing conglomerates the highest abundance of them. The permeability produced by open stylolites in conglomerates of the Oliana anticline cannot be calculated precisely because stylolite planes are misoriented and wholly or partially filled by calcite cement and accumulations of insoluble minerals. In the case of sandstones, stylolites are less abundant and they are often closed, thus the permeability associated with stylolites in them is expected to be low.

In contrast to stylolites, the fracturing of the detrital succession in the Oliana anticline should improve the overall permeability of this analogue (Fig. 14). Permeability through fractures and fault systems has been reported to be two orders of magnitude higher than the matrix permeability of the rocks (Evans et al., 1997; Rawling et al., 2001; Faulds et al., 2011; Meier et al., 2015; Muñoz-López et al., 2022).

The effect of open fractures on the porosity and permeability of conglomerates and sandstones has been widely discussed above. Open fractures are more abundant in the southern limb, however, they are widely spaced and formed by a few fracture families (F4 and F5). Based

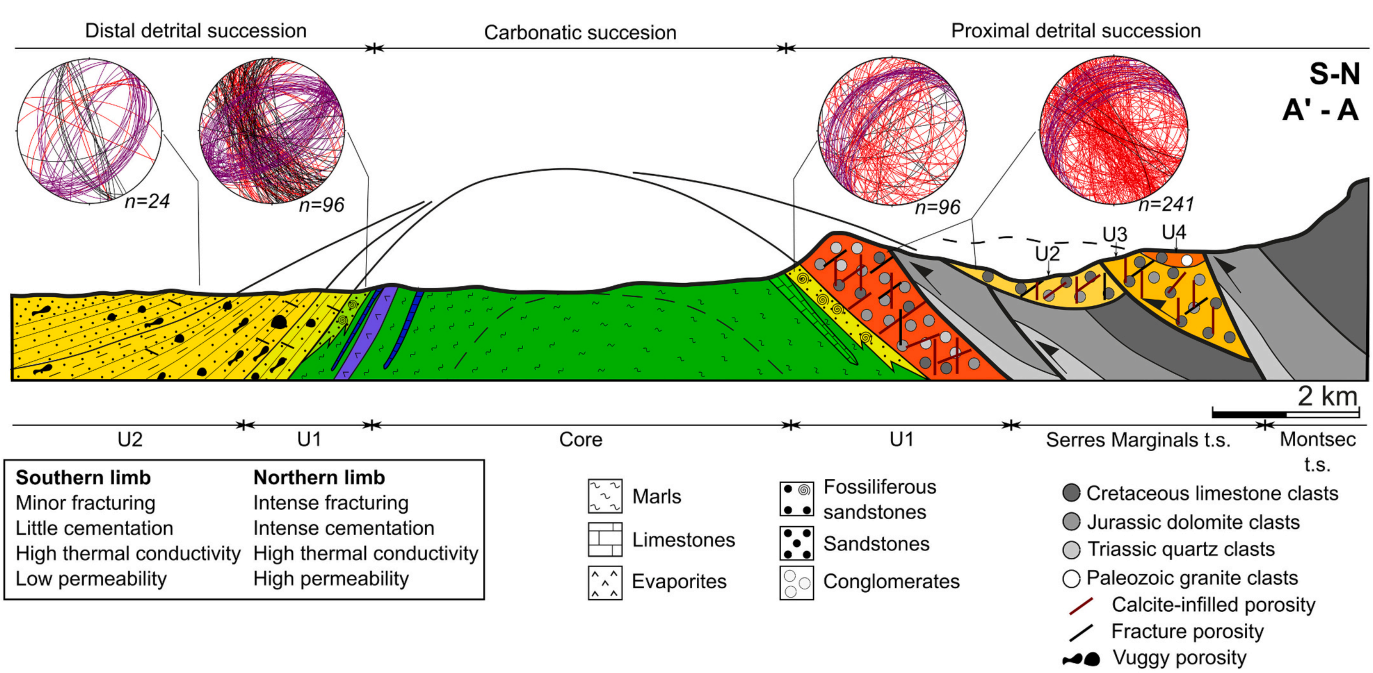

Fig. 14. Summary of the thermal conductivity in Oliana anticline. According to the results shown in Figs. 8, 10 and 13, there is no direct correlation between the petrophysical and the petrothermal properties of the rocks in the Oliana anticline. Instead, compositional control on thermal conductivity is suggested. The figure displays the different sedimentary successions in Oliana. The thermal conductivity legend is shown in Fig. 13. A standard value of 2.5 Wm^{-1} K^{-1} is used for the marls of the core, low conductivity values are measured in the carbonates and evaporites, whereas the measured conductivities are higher for the detrital succession. Stereoplots are also shown to visualize the potential fracture permeability of the anticline in combination with the conductivity of the rocks. The most relevant porosity types and geological characteristics are also displayed in the figure.

on these characteristics, fracture permeability is expected to increase towards the south of the Oliana anticline, although more studies are needed to improve the assessment of the fracture connectivity in this sector of the fold. The other structural areas (i.e., the northern limb and the NE closure) are more challenging to model because several fractures within systems F1, F2, F3 and F6 affect these zones (according to Sussman et al., 2004). Moreover, the permeability of the northern limb should be lower than in the southern limb because most of the fractures in this area are calcite cemented. The NE closure shows an intermediate situation with some calcite cemented fractures and some open fractures.

Although the matrix permeability in the Oliana anticline does not allow us to classify this structure as a good geothermal reservoir, additional studies can assess the potential of this area as a CO_2 storage site. For instance, Sun et al. (2021a) reviewed the nearby Puig-Reig anticline, which represents the eastern lateral equivalent of the Oliana anticline in the Southern Pyrenees, as an analogue for CO_2 storage. The results of this research can be applied to the data of Oliana, as they are based on a similar structure (i.e., an anticlinal fold located at the external part of the South Pyrenean fold-and-thrust belt) and facies (i.e., detrital rocks of fluvial and alluvial successions). Thus, the low permeabilities and high porosities measured throughout the lithic and hybrid arenites facies at the southern limb of the anticline would be an exciting subject for studying this structure as an outcrop analogue for CO_2 storage potential, which is an ongoing study.

9. Conclusions

In this contribution, we present the petrophysical and petrothermal characterization of the Oliana anticline based on the petrological, petrophysical and petrothermal analysis of 52 samples and 63 thin sections from the five principal sedimentary facies (Fa-1 to Fa-5): conglomerates, hybrid arenites, lithic arenites, carbonates and evaporites.

The petrophysical properties of 40 samples have been studied in 36 bed-parallel plugs and 26 bed-perpendicular plugs. The petrophysical results of the anticline show that:

1. There is a slight mineral density variation (2.334–2.767 g/cm^3) in the analysed rocks, indicating that the composition of samples is almost homogeneous throughout the anticline.
2. Bulk density (2.107–2.710 g/cm^3), connected porosity (0.42–22.14%), permeability (0.001–393 mD) and P-wave velocity (2236–6322 ms^{-1}) of rocks are highly heterogeneous. Comparing petrophysical variables establishes a slight negative correlation between P-wave velocity and connected porosity.

Petrophysical results reveal that total porosity and pore-space geometry are the main factors modifying the rest of the petrophysical variables. The formation of porosity in the Oliana anticline is widely influenced by the tectonic, burial and diagenetic history of the rocks. Thereby, fracturing, dissolution and cementation are recognized to be the principal processes enhancing or decreasing porosity. In turn, an intense structural control on these properties has been observed since the most fractured and cemented parts of the anticline are located at the NE closure and the northern limb of the fold, near the Serres Marginals and Montsec thrust sheets. A petrological control on dissolution is proposed, as the facies displaying higher micrite content (i.e., hybrid arenites, greywackes within lithic arenites and matrix-supported carbonates) present more vuggy porosity. However, for the same sedimentary facies, changes in porosity depend on the structural position of the samples; in such cases, a structural control over dissolution cannot be ruled out.

In this study, matrix permeability and connected porosity are not correlated. The permeability of rocks is strongly dependent on pore geometry and, consequently, on the porosity-forming mechanism, being enhanced in fracture and stylolite porosity and reduced in isolated vuggy porosity. The northern limb of the anticline is shown to be the most permeable zone, whereas the southern limb is the less permeable region of the fold. This result matches the principal type of porosity observed in the dominant sedimentary facies of these structural zones (conglomerates and hybrid arenites, respectively).

The petrothermal properties of 35 samples have been studied in 24 bed-parallel plugs and 31 bed-perpendicular plugs. The petrothermal results of the anticline show that:

1. Thermal conductivity is higher for detrital sedimentary facies (Fa-1 to Fa-3, 3.0–3.646 Wm^{-1} K^{-1}) than for carbonates and evaporites (Fa-4 and Fa-5 respectively, 1.846–3.232 Wm^{-1} K^{-1}). Consequently, a high-conductive region is formed in the limbs of the Oliana anticline, whereas the core of the structure represents a low-conductive zone.
2. Thermal conductivity displays a slight positive correlation with the mineral density of rocks. Neither bulk density, porosity, permeability nor P-wave velocity are correlated to thermal conductivity.
3. The differences in thermal conductivity of the rocks within the detrital succession of the anticline are strictly linked to little compositional changes between rocks of different tectonosedimentary units. Indeed, the most conductive tectonosedimentary units are Units 1 and 4, whose rocks present a high percentage of high-conductive materials such as Compostela hyacinths from the Keuper facies and dolomite clasts from the Jurassic strata, both cropping out at the Serres Marginals thrust sheets, and granite and quartz clasts coming from the erosion of the Axial Pyrenean Zone. Rocks from tectonosedimentary Units 2 and 3 are less conductive than those of Units 1 and 4 and are rich in carbonate clasts from the erosion of the Cretaceous strata outcropping at the adjacent Montsec and Serres Marginals thrust sheets and the more distant Bóixols thrust sheet.

Based on the permeability and the thermal conductivity measured in rocks of the Oliana anticline, the structure is classified as a petrothermal system in which the convective movement of fluids will be avoided because of the limited reservoir permeability. Thus, we conclude that the Oliana anticline would not be a good geothermal reservoir because of its low permeability. However, it has potential properties for assessing CO_2 storage potential, which is ongoing research.

Declaration of Competing Interest

The authors declare that they have no known competing financial interests or personal relationships that could have appeared to influence the work reported in this paper.

Data availability

Data used in the article is included in the data tables within Supplementary material.

Acknowledgements

This research was performed within the framework of DGICYT Spanish Project PGC2018-093903-B-C22 and PID2021-12246NB-C22 Ministerio de Ciencia, Innovación y Universidades/Agencia Estatal de Investigación/Fondo Europeo de Desarrollo Regional and the Catalan Council to the Grup de Recerca Reconegut Geologia Sedimentària (2021 SGR-Cat 00349).

DC acknowledges the Spanish Ministry of Science and Innovation for the "Juan de la Cierva Formación" fellowship FJC2020-043488-I AEI/10.13039/501100011033.

PR acknowledges the Universitat de Barcelona and Repsol Exploración. S.A. for the "Repsol-UB 2020" fellowship D/226000900/C2022A/G00/ PDZJK002 and the Universitat de Barcelona for the "PREDOC-UB 2020" fellowship.

Authors acknowledge Elisabet Beamud and Eduard Roca of the Universitat de Barcelona for their help interpreting the Oliana anticline chronostratigraphy. We also want to acknowledge the two anonymous reviewers for their advice and corrections on the original manuscript.

Appendix A. Supplementary data

Supplementary data to this article can be found online at https://doi.org/10.1016/j.gloplacha.2023.104057.

References

Abdulagatova, Z., Abdulagatov, I.M., Emirov, V.N., 2009. Effect of temperature and pressure on the thermal conductivity of sandstone. Int. J. Rock Mech. Min. Sci. 46, 1055–1071. https://doi.org/10.1016/j.ijrmms.2009.04.011.
Al-Dousari, M., Garrouch, A.A., Al-Omair, O., 2016. Investigating the dependence of shear wave velocity on petrophysical parameters. J. Pet. Sci. Eng. 146, 286–296. https://doi.org/10.1016/j.petrol.2016.04.036.
Aretz, A., Bär, K., Götz, A.E., Sass, I., 2015. Outcrop analogue study of Permocarboniferous geothermal sandstone reservoir formations (northern Upper Rhine Graben, Germany): impact of mineral content, depositional environment and diagenesis on petrophysical properties. Int. J. Earth Sci. 105, 1431–1452. https://doi.org/10.1007/s00531-015-1263-2.
Bauer, J.F., Meier, S., Philipp, S.L., 2015. Architecture, fracture system, mechanical properties and permeability structure of a fault zone in Lower Triassic sandstone, Upper Rhine Graben. Tectonophysics 647–648, 132–145. https://doi.org/10.1016/J.TECTO.2015.02.014.
Bauer, J.F., Krumbholz, M., Meier, S., Tanner, D.C., 2017. Predictability of properties of a fractured geothermal reservoir: the opportunities and limitations of an outcrop analogue study. Geothermal Energy 5. https://doi.org/10.1186/s40517-017-0081-0.
Beaumont, C., Muñoz, J.A., Hamilton, J., Fullsack, P., 2000. Factors controlling the Alpine evolution of the central Pyrenees inferred from a comparison of observations and geodynamical models. Journal of Geophysical Research: Solid Earth 105, 8121–8145. https://doi.org/10.1029/1999JB900390.
Bell, F.G., 1978. Petrographical factors relating to porosity and permeability in the Fell Sandstone. Q. J. Eng. Geol. Hydrogeol. 11, 113–126. https://doi.org/10.1144/GSL.QJEG.1978.011.02.01.
Bell, F.G., Culshaw, M.G., 1998. Petrographic and engineering properties of sandstones from the Sneinton Formation, Nottinghamshire, England. Q. J. Eng. Geol. Hydrogeol. 31, 5–19. https://doi.org/10.1144/GSL.QJEG.1998.031.P1.02.
Beyer, D., Kunkel, C., Aehnelt, M., Pudlo, D., Voigt, T., Nover, G., Gaupp, R., 2014. Influence of depositional environment and diagenesis on petrophysical properties of clastic sediments (Buntsandstein of the Thuringian Syncline, Central Germany). Z. Dtsch. Ges. Geowiss. 165, 345–365. https://doi.org/10.1127/1860-1804/2014/0072.
Birch, A.F., Clark, H., 1940. The thermal conductivity of rocks and its dependence upon temperature and composition. Am. J. Sci. 238, 529–558. https://doi.org/10.2475/AJS.238.8.529.
Bitzer, K., Trave, A., Carmona, J.M., Calvet, F., 1998. Fluid flow in foreland basins during emplacement of thrust sheets; modelling the South-Pyrenean Ainsa Basin. Bulletin de la Societé Géologique de France 169, 627–633.
Bjørlykke, K., Ramm, M., Saigal, G., 1989. Sandstone diagenesis and porosity modification during basin evolution. Geol. Rundsch. 78, 243–268. https://doi.org/10.1007/BF01988363.
Bohnsack, D., Potten, M., Pfrang, D., Wolpert, P., Zosseder, K., 2020. Porosity–permeability relationship derived from Upper Jurassic carbonate rock cores to assess the regional hydraulic matrix properties of the Malm reservoir in the South German Molasse Basin. Geothermal Energy 8. https://doi.org/10.1186/s40517-020-00166-9.
Breeze, P., 2019. Power Generation Technologies, 3rd ed. Elsevier.
Brigaud, F., Vasseur, G., 1989. Mineralogy, porosity and fluid control on thermal conductivity of sedimentary rocks. Geophys. J. 98, 525–542. https://doi.org/10.1111/j.1365-246X.1989.tb02287.x.
Burbank, D.W., Vergés, J., 1994. Reconstruction of topography and related depositional systems during active thrusting. J. Geophys. Res. 99, 281–297. https://doi.org/10.1029/94JB00463.
Burbank, D.W., Puigdefàbregas, C., Muñoz, J., 1992. The chronology of the Eocene tectonic and stratigraphic development of the eastern Pyrenean foreland basin, Northeast Spain. Geol. Soc. Am. Bull. 104, 1101–1120. https://doi.org/10.1130/0016-7606(1992)104<1101:TCOTET>2.3.CO;2.
Cámara, P., Flinch, J.F., 2017. The Southern Pyrenees, in: Permo-Triassic Salt Provinces of Europe, North Africa and the Atlantic Margins. Elsevier, pp. 395–415. https://doi.org/10.1016/b978-0-12-809417-4.00019-7.
Carcione, J.M., Gei, D., Yu, T., Ba, J., 2019. Effect of Clay and Mineralogy on Permeability. Pure Appl. Geophys. 176, 2581–2594. https://doi.org/10.1007/s00024-019-02117-3.
Cascella, A., Dinarès-Turell, J., 2009. Integrated calcareous nannofossil biostratigraphy and magnetostratigraphy from the uppermost marine Eocene deposits of the southeastern Pyrenean foreland basin: Evidences for marine Priabonian deposition. Geol. Acta 7 (1–2), 281–296. https://doi.org/10.1344/105.000000282.
Cavailhes, T., Sizun, J.P., Labaume, P., Chauvet, A., Buatier, M., Soliva, R., Mezri, L., Charpentier, D., Leclere, H., Trave, A., Gout, C., 2013. Influence of fault rock foliation on fault zone permeability: the case of deeply buried arkosic sandstones (Grès d'Annot, southeastern France). AAPG Bull. 97, 1521–1543. https://doi.org/10.1306/03071312127.
Čermák, V., Rybach, L., 1989. Vertical distribution of heat production in the continental crust. Tectonophysics 159, 217–230. https://doi.org/10.1016/0040-1951(89)90129-7.
Chabani, A., Trullenque, G., Ledésert, B.A., Klee, J., 2021. Multiscale Characterization of Fracture Patterns: a Case Study of the Noble Hills Range (Death Valley, CA, USA). Application to Geothermal Reservoirs. Geosciences (Basel) 11, 280. https://doi.org/10.3390/GEOSCIENCES11070280.
Choukroune, P., 1989. The Ecors Pyrenean deep seismic profile reflection data and the overall structure of an orogenic belt. Tectonics 8, 23–39. https://doi.org/10.1029/TC008I001P00023.
Clark, S.P., 1966. Handbook of Physical Constants, GSA Memoirs. Geological Society of America. https://doi.org/10.1130/MEM97.
Clauser, C., Huenges, E., 1995. Thermal conductivity of rocks and minerals. In: Rock Physics and Phase Relations A Handbook of Physical Constant. Geological Society of America, pp. 105–126. https://doi.org/10.1029/rf003p0105.
Cofrade, G., Cantarero, I., Gratacós, Ó., Ferrer, O., Ramirez-Perez, P., Travé, A., Roca, E., 2023. Allochthonous salt advance recorded by the adjacent syn-kinematic sedimentation: example from the Les Avellanes diapir (South Central Pyrenees). Glob. Planet. Chang. 220, 104020 https://doi.org/10.1016/j.gloplacha.2022.104020.
Costa, E., Garcés, M., López-Blanco, M., Beamud, E., Gómez-Paccard, M., Larrasoaña, J.C., 2010. Closing and continentalization of the South Pyrenean foreland basin (NE Spain): magnetochronological constraints. Basin Res. 22, 904–917. https://doi.org/10.1111/J.1365-2117.2009.00452.X.
Cruset, D., Cantarero, I., Travé, A., Vergés, J., John, C.M., 2016. Crestal graben fluid evolution during growth of the Puig-reig anticline (South Pyrenean fold and thrust belt). J. Geodyn. 101, 30–50. https://doi.org/10.1016/j.jog.2016.05.004.
Cruset, D., Cantarero, I., Vergés, J., John, C.M., Muñoz-López, D., Travé, A., 2018. Changes in fluid regime in syn-orogenic sediments during the growth of the south Pyrenean fold and thrust belt. Glob. Planet. Chang. 171, 207–224. https://doi.org/10.1016/J.GLOPLACHA.2017.11.001.
Cruset, D., Vergés, J., Albert, R., Gerdes, A., Benedicto, A., Cantarero, I., Travé, A., 2020. Quantifying deformation processes in the SE Pyrenees using U–Pb dating of fracture-filling calcites. J. Geol. Soc. Lond. 177, 1186–1196. https://doi.org/10.1144/JGS2020-014.
Di Sipio, E., Chiesa, S., Destro, E., Galgaro, A., Giaretta, A., Gola, G., Manzella, A., 2013. Rock thermal Conductivity as Key Parameter for Geothermal Numerical Models. Energy Procedia 40, 87–94. https://doi.org/10.1016/J.EGYPRO.2013.08.011.
Duwiquet, H., Guillou-Frottier, L., Arbaret, L., Guillon, T., Bellanger, M., Heap, M.J., 2020. Crustal Fault Zone: New geothermal reservoir? Structural dataset and preliminary 3D TH(M) modelling of the Pontgibaud fault zone (French Massif Central). In: PROCEEDINGS, 45th Workshop on Geothermal Reservoir Engineering, pp. 1–11.
Eberhart-Phillips, D., Han, D.H., Zoback, M.D., 1989. Empirical relationships among seismic velocity, effective pressure, porosity, and clay content in sandstone. Geophysics 54, 13–130. https://doi.org/10.1190/1.1442580.
Ehrenberg, S.N., Walderhaug, O., 2015. Preferential Calcite Cementation of Macropores in Microporous Limestones. J. Sediment. Res. 85, 780–793. https://doi.org/10.2110/JSR.2015.52.
Ehrenberg, S.N., Morad, S., Yaxin, L., Chen, R., 2016. Stylolites and Porosity in a Lower Cretaceous Limestone Reservoir, Onshore Abu Dhabi, U.A.E. J. Sediment. Res. 86, 1228–1247. https://doi.org/10.2110/JSR.2016.68.
El Sayed, N.A., Abuseda, H., Kassab, M.A., 2015. Acoustic wave velocity behavior for some Jurassic carbonate samples, north Sinai, Egypt. Journal of African Earth Sciences 111, 14–25. https://doi.org/10.1016/j.jafrearsci.2015.07.016.
Evans, J.P., Forster, C.B., Goddard, J., 1997. Permeability of fault-related rocks, and implications for hydraulic structure of fault zones. J. Struct. Geol. 19, 1393–1404. https://doi.org/10.1016/S0191-8141(97)00057-6.
Farrell, N.J.C., Healy, D., 2017. Anisotropic pore fabrics in faulted porous sandstones. J. Struct. Geol. 104, 125–141. https://doi.org/10.1016/j.jsg.2017.09.010.
Farrell, N.J.C., Healy, D., Taylor, C.W., 2014. Anisotropy of permeability in faulted porous sandstones. J. Struct. Geol. 63, 50–67. https://doi.org/10.1016/j.jsg.2014.02.008.
Faulds, J.E., Hinz, N.H., Coolbaugh, M.F., Cashman, P.H., Kratt, C., Dering, G., Edwards, J., Mayhew, B., McLachlan, H., 2011. Assessment of favorable structural settings of geothermal systems in the Great Basin, Western USA. Transactions - Geothermal Resources Council. 777–783.
Faulds, J.E., Hinz, N.H., Coolbaugh, M.F., Depolo, C.M., Siler, D.L., Shevenell, L.A., Hammond, W.C., Kreemer, C., Queen, J.H., 2016. Discovering Geothermal Systems in the Great Basin Region: An Integrated Geologic, Geochemical, and Geophysical Approach for Establishing Geothermal Play Fairways. In: PROCEEDINGS, 41st Workshop on Geothermal Reservoir Engineering, pp. 1–15.
Fjeldskaar, W., Christie, O.H.J., Midttømme, K., Virnovsky, G., Jensen, N.B., Lohne, A., Eide, G.I., Balling, N., 2009. On the determination of thermal conductivity of sedimentary rocks and the significance for basin temperature history. Pet. Geosci. 15, 367–380. https://doi.org/10.1144/1354-079309-814.
Fuchs, S., Schütz, F., Förster, H.J., Förster, A., 2013. Evaluation of common mixing models for calculating bulk thermal conductivity of sedimentary rocks: Correction charts and new conversion equations. Geothermics 47, 40–52. https://doi.org/10.1016/j.geothermics.2013.02.002.
Garcés, M., López-Blanco, M., Valero, L., Beamud, E., Muñoz, J.A., Oliva-Urcia, B., Vinyoles, A., Arbués, P., Cabello, P., Cabrera, L., 2020. Paleogeographic and

sedimentary evolution of the South Pyrenean foreland basin. Mar. Pet. Geol. 113, 104105 https://doi.org/10.1016/J.MARPETGEO.2019.104105.
Garia, S., Pal, A.K., Ravi, K., Nair, A.M., 2019. A comprehensive analysis on the relationships between elastic wave velocities and petrophysical properties of sedimentary rocks based on laboratory measurements. Journal of Petroleum Exploration and Production Technology 9, 1869–1881. https://doi.org/10.1007/s13202-019-0675-0.
Ghanizadeh, A., Clarkson, C.R., Aquino, S., Ardakani, O.H., Sanei, H., 2015. Petrophysical and geomechanical characteristics of Canadian tight oil and liquid-rich gas reservoirs: I. Pore network and permeability characterization. Fuel 153, 664–681. https://doi.org/10.1016/j.fuel.2015.03.020.
Gomez-Rivas, E., Martín-Martín, J.D., Bons, P.D., Koehn, D., Griera, A., Travé, A., Llorens, M.G., Humphrey, E., Neilson, J., 2022. Stylolites and stylolite networks as primary controls on the geometry and distribution of carbonate diagenetic alterations. Mar. Pet. Geol. 136 https://doi.org/10.1016/j.marpetgeo.2021.105444.
Götz, A.E., Lenhardt, N.S., 2011. The Anisian carbonate ramp system of Central Europe (Peri-Tethys Basin): sequences and reservoir characteristics. Acta Geol. Pol. 61, 59–70.
Haffen, S., Géraud, Y., Rosener, M., Diraison, M., 2017. Thermal conductivity and porosity maps for different materials: a combined case study of granite and sandstone. Geothermics 66, 143–150. https://doi.org/10.1016/j.geothermics.2016.12.005.
Hang, X., Zhang, H., Guo, J., Li, J., Fang, T., 2022. Controlling factors on elastic wave velocities of conglomerate – Experimental and theoretical study. J. Pet. Sci. Eng. 209 https://doi.org/10.1016/j.petrol.2021.109837.
Heap, M.J., Kushnir, A.R.L., Gilg, H.A., Wadsworth, F.B., Reuschlé, T., Baud, P., 2017. Microstructural and petrophysical properties of the Permo-Triassic sandstones (Buntsandstein) from the Soultz-sous-Forêts geothermal site (France). Geothermal Energy 5. https://doi.org/10.1186/s40517-017-0085-9.
Heap, M.J., Kushnir, A.R.L., Gilg, H.A., Violay, M.E.S., Harlé, P., Baud, P., 2019. Petrophysical properties of the Muschelkalk from the Soultz-sous-Forêts geothermal site (France), an important lithostratigraphic unit for geothermal exploitation in the Upper Rhine Graben. Geothermal Energy 7. https://doi.org/10.1186/s40517-019-0145-4.
Hinz, N.H., Faulds, J.E., Siler, D.L., Tobin, B., Blake, K., Tiedeman, A., Sabin, A., Blankenship, D., Kennedy, M., Rhodes, G., Nordquist, J., Hickman, S., Glen, J., Williams, C., Robertson-Tait, A., Calvin, W., 2016. Stratigraphic and Structural Framework of the Proposed Farallon Site, Nevada. In: PROCEEDINGS, 41st Workshop on Geothermal Reservoir Engineering, pp. 1–12.
Homuth, S., Sass, I., 2014. Outcrop Analogue vs. Reservoir Data: Characteristics and Controlling Factors of Physical Properties of the Upper Jurassic Geothermal Carbonate Reservoirs of the Molasse Basin, Germany. In: PROCEEDINGS, 38th Workshop on Geothermal Reservoir Engineering, pp. 1–10.
Homuth, S., Götz, A.E., Sass, I., 2011. Outcrop Analogue Studies for Reservoir Characterization of Deep Geothermal Systems in Upper Jurassic Limestone Formations (South Germany). In: AAPG International Conference and Exhibition.
Homuth, S., Götz, A.E., Sass, I., 2015a. Physical Properties of the Geothermal Carbonate Reservoirs of the Molasse Basin, Germany-Outcrop Analogue vs. Reservoir Data Pre-Drakensberg volcanism and sill intrusions of the South African Karoo Supergroup and their significance for basin evolution View project Heat dissipation of buried energy cable systems View project Physical Properties of the Geothermal Carbonate Reservoirs of the Molasse Basin, Germany-Outcrop Analogue vs. Reservoir Data. In: Proceedings World Geothermal Congress, pp. 1–11.
Homuth, S., Götz, A.E., Sass, I., 2015b. Reservoir characterization of the Upper Jurassic geothermal target formations (Molasse Basin, Germany): role of thermofacies as exploration tool. Geothermal Energy Science 3, 41–49. https://doi.org/10.5194/GTES-3-41-2015.
Horai, K., 1971. Thermal conductivity of rock-forming minerals. J. Geophys. Res. 76, 1278–1308. https://doi.org/10.1029/jb076i005p01278.
Houseknecht, D.W., 1987. Assessing the Relative Importance of Compaction Processes and Cementation to Reduction of Porosity in Sandstones. AAAPG Bulletin 71, 633–642. https://doi.org/10.1306/9488787F-1704-11D7-8645000102C1865D.
Houseknecht, D.W., 1988. Intergranular pressure solution in four Quartzose Sandstones. J. Sediment. Petrol. 58, 228–246. https://doi.org/10.1306/212F8D64-2B24-11D7-8648000102C1865D.
Howell, J.A., Martinius, A.W., Good, T.R., 2014. The application of outcrop analogues in geological modelling: a review, present status and future outlook. Geol. Soc. Lond., Spec. Publ. 387, 1–25. https://doi.org/10.1144/sp387.12.
Huenges, E., 2010. Geothermal Energy Systems: Exploration, Development, and Utilization. Wiley, Weinheim.
Humphrey, E., Gomez-Rivas, E., Koehn, D., Bons, P.D., Neilson, J., Martín-Martín, J.D., Schoenherr, J., 2019. Stylolite-controlled diagenesis of a mudstone carbonate reservoir: a case study from the Zechstein_2_Carbonate (Central European Basin, NW Germany). Mar. Pet. Geol. 109, 88–107. https://doi.org/10.1016/j.marpetgeo.2019.05.040.
Iyare, U.C., Ramsook, R., Blake, O.O., Faulkner, D.R., 2020. Petrographical and petrophysical characterization of the late cretaceous Naparima Hill Formation, Central Range, Trinidad, West Indies. Int. J. Coal Geol. 230 https://doi.org/10.1016/j.coal.2020.103592.
Kaminskaite, I., Piazolo, S., Emery, A.R., Shaw, N., Fisher, Q.J., 2022. The Importance of Physiochemical Processes in Decarbonisation Technology Applications Utilizing the Subsurface: a Review. Earth Science, Systems and Society 0, 8. https://doi.org/10.3389/ESSS.2022.10043.
Kushnir, A.R.L., Heap, M.J., Baud, P., Gilg, H.A., Reuschlé, T., Lerouge, C., Dezayes, C., Duringer, P., 2018. Characterizing the physical properties of rocks from the Paleozoic to Permo-Triassic transition in the Upper Rhine Graben. Geothermal Energy 6. https://doi.org/10.1186/s40517-018-0103-6.
Labus, M., Labus, K., 2018. Thermal conductivity and diffusivity of fine-grained sedimentary rocks. J. Therm. Anal. Calorim. 132, 1669–1676. https://doi.org/10.1007/S10973-018-7090-5/FIGURES/3.
Lacroix, B., Travé, A., Buatier, M., Labaume, P., Vennemann, T., Dubois, M., 2014. Syntectonic fluid-flow along thrust faults: example of the South-Pyrenean fold-and-thrust belt. Mar. Pet. Geol. 49, 84–98. https://doi.org/10.1016/j.marpetgeo.2013.09.005.
Laronne Ben-Itzhak, L., Aharonov, E., Karcz, Z., Kaduri, M., Toussaint, R., 2014. Sedimentary stylolite networks and connectivity in limestone: Large-scale field observations and implications for structure evolution. J. Struct. Geol. 63, 106–123. https://doi.org/10.1016/j.jsg.2014.02.010.
Luo, M., Wood, J.R., Cathles, L.M., 1994. Prediction of thermal conductivity in reservoir rocks using fabric theory. J. Appl. Geophys. 32, 321–334. https://doi.org/10.1016/0926-9851(94)90031-0.
Martín-Martín, J.D., Gomez-Rivas, E., Gómez-Gras, D., Travé, A., Ameneiro, R., Koehn, D., Bons, P.D., 2018. Activation of stylolites as conduits for overpressured fluid flow in dolomitized platform carbonates. Geol. Soc. Lond., Spec. Publ. 459, 157–176. https://doi.org/10.1144/SP459.3.
Mckenna, T.E., Sharp Jr., J., Lynch, L.F., 1996. Thermal conductivity of Wilcox and Frio Sandstones in South Texas (Gulf of Mexico Basin). AAPG Bull. 80, 1203–1215. https://doi.org/10.1306/64ED8CE6-1724-11D7-8645000102C1865D.
Meier, S., Bauer, J.F., Philipp, S.L., 2015. Fault zone characteristics, fracture systems and permeability implications of Middle Triassic Muschelkalk in Southwest Germany. J. Struct. Geol. 70, 170–189. https://doi.org/10.1016/j.jsg.2014.12.005.
Meigs, A.J., Burbank, D.W., 1997. Growth of the South Pyrenean orogenic wedge. Tectonics 16, 239–258. https://doi.org/10.1029/96TC03641.
Meigs, A.J., Vergés, J., Burbank, D.W., 1996. Ten-million-year history of a thrust sheet. GSA Bull. 108, 1608–1625. https://doi.org/10.1130/0016-7606(1996)108<1608:TMYHOA>2.3.CO;2.
Midttømme, K., Roaldset, E., 1998. The effect of grain size on thermal conductivity of quartz sands and silts. Pet. Geosci. 4, 165–172. https://doi.org/10.1144/petgeo.4.2.165.
Mielke, P., Bignall, G., Sass, I., 2010. Permeability and thermal conductivity measurements of near surface units at the wairakei geothermal field, New Zealand. In: PROCEEDINGS World Geothermal Congress 2010, pp. 1–7.
Mielke, P., Nehler, M., Bignall, G., Sass, I., 2015. Thermo-physical rock properties and the impact of advancing hydrothermal alteration - a case study from the Tauhara geothermal field, New Zealand. J. Volcanol. Geotherm. Res. 301, 14–28. https://doi.org/10.1016/j.jvolgeores.2015.04.007.
Mielke, P., Bär, K., Sass, I., 2017. Determining the relationship of thermal conductivity and compressional wave velocity of common rock types as a basis for reservoir characterization. J. Appl. Geophys. 140, 135–144. https://doi.org/10.1016/j.jappgeo.2017.04.002.
Moeck, I.S., 2014. Catalog of geothermal play types based on geologic controls. Renew. Sust. Energ. Rev. 37, 867–882. https://doi.org/10.1016/j.rser.2014.05.032.
Morad, D., Nader, F.H., Gasparrini, M., Morad, S., Rossi, C., Marchionda, E., Al Darmaki, F., Martines, M., Hellevang, H., 2018a. Comparison of the diagenetic and reservoir quality evolution between the anticline crest and flank of an Upper Jurassic carbonate gas reservoir, Abu Dhabi, United Arab Emirates. Sediment. Geol. 367, 96–113. https://doi.org/10.1016/J.SEDGEO.2018.02.008.
Morad, D., Nader, F.H., Morad, S., Darmaki, F.A.L., Hellevang, H., 2018b. Impact of Stylolitization On Fluid Flow and Diagenesis in Foreland Basins: evidence from an Upper Jurassic Carbonate Gas Reservoir, Abu Dhabi, United Arab Emirates. J. Sediment. Res. 88, 1345–1361. https://doi.org/10.2110/JSR.2018.70.
Morad, D., Paganoni, M., Al Harthi, A., Morad, S., Ceriani, A., Mansurbeg, H., al Suwaidi, A., Al-Aasm, I.S., Ehrenberg, S.N., 2018c. Origin and evolution of microporosity in packstones and grainstones in a Lower Cretaceous carbonate reservoir, United Arab Emirates. Geol. Soc. Lond., Spec. Publ. 435, 47–66. https://doi.org/10.1144/SP435.20.
Morad, S., Al Suwaidi, M., Mansurbeg, H., Morad, D., Ceriani, A., Paganoni, M., Al-Aasm, I., 2019. Diagenesis of a limestone reservoir (Lower Cretaceous), Abu Dhabi, United Arab Emirates: Comparison between the anticline crest and flanks. Sediment. Geol. 380, 127–142. https://doi.org/10.1016/J.SEDGEO.2018.12.004.
Müller, C., Siegesmund, S., Blum, P., 2010. Evaluation of the representative elementary volume (REV) of a fractured geothermal sandstone reservoir. Environ. Earth Sci. 61, 1713–1724. https://doi.org/10.1007/s12665-010-0485-7.
Muñoz, J.A., 1992. Evolution of a continental collision belt: ECORS-Pyrenees crustal balanced cross-section. In: McClay, K.R. (Ed.), Thrust Tectonics. Springer, Dordrecht.
Muñoz, J.A., 2002. The Pyrenees. In: Gibbons, W., Moreno, T. (Eds.), The Geology of Spain. Geological Society, pp. 370–385.
Muñoz-López, D., Alías, G., Cruset, D., Cantarero, I., John, C.M., Travé, A., 2020a. Influence of basement rocks on fluid evolution during multiphase deformation: the example of the Estamariu thrust in the Pyrenean Axial Zone. Solid Earth 11, 2257–2281. https://doi.org/10.5194/SE-11-2257-2020.
Muñoz-López, D., Cruset, D., Cantarero, I., Benedicto, A., John, C.M., Travé, A., 2020b. Fluid Dynamics in a Thrust Fault Inferred from Petrology and Geochemistry of Calcite Veins: an example from the Southern Pyrenees. Geofluids. https://doi.org/10.1155/2020/8815729.
Muñoz-López, D., Cruset, D., Vergés, J., Cantarero, I., Benedicto, A., Mangenot, X., Albert, R., Gerdes, A., Beranoaguirre, A., Travé, A., 2022. Spatio-temporal variation of fluid flow behavior along a fold: the Bóixols-Sant Corneli anticline (Southern Pyrenees) from U–Pb dating and structural, petrographic and geochemical constraints. Marine and Petroleum Geology 143. https://doi.org/10.1016/j.marpetgeo.2022.105788. Article 105788.

Mutti, E., Rosell, J., Allen, G.P., Fonnesu, F., Sgavetti, M., 1985. The Eocene Bartonia tide dominated delta-shelf system in the Ager basin. In: Guidebook for the 6th European Regional Meeting 576–600.

Nardini, N., Muñoz-López, D., Cruset, D., Cantarero, I., Martín-Martín, J.D., Benedicto, A., Gomez-Rivas, E., John, C.M., Travé, A., 2019. From early contraction to post-folding fluid evolution in the frontal part of the bóixols thrust sheet (Southern Pyrenees) as revealed by the texture and geochemistry of calcite cements. Minerals 9. https://doi.org/10.3390/min9020117.

Oliver, J., 1986. Fluids expelled tectonically from orogenic belts: their role in hydrocarbon migration and other geologic phenomena. Geology 14, 99–102. https://doi.org/10.1130/0091-7613(1986)14<99:FETFOB>2.0.CO;2.

Paganoni, M., Al Harthi, A., Morad, D., Morad, S., Ceriani, A., Mansurbeg, H., Al Suwaidi, A., Al-Aasm, I.S., Ehrenberg, S.N., Sirat, M., 2016. Impact of stylolitization on diagenesis of a lower cretaceous carbonate reservoir from a giant oilfield, Abu Dhabi, United Arab Emirates. Sediment. Geol. 335, 70–92. https://doi.org/10.1016/J.SEDGEO.2016.02.004.

Popov, Y., Pohl, J., Romushkevich, R., Tertychnyi, V., Soffel, H., 2003. Geothermal characteristics of the Ries impact structure. Geophys. J. Int. 154, 355–378. https://doi.org/10.1046/j.1365-246X.2003.01925.x.

Puigdefàbregas, C., Souquet, P., 1986. Tecto-sedimentary cycles and depositional sequences of the Mesozoic and Tertiary from the Pyrenees. Tectonophysics 129, 173–203. https://doi.org/10.1016/0040-1951(86)90251-9.

Puigdefàbregas, C., Muñoz, J.A., Marzo, M., 1986. Thrust Belt Development in the Eastern Pyrenees and Related Depositional Sequences in the Southern Foreland Basin. In: Allen, A., Homewood, P. (Eds.), Foreland Basins. Blackwell, Oxford, pp. 229–246. https://doi.org/10.1002/9781444303810.CH12.

Rawling, G.C., Goodwin, L.B., Wilson, J.L., 2001. Internal architecture, permeability structure, and hydrologic significance of contrasting fault-zone types. Geology 29, 43–46. https://doi.org/10.1130/0091-7613(2001)029<0043:IAPSAH>2.0.CO;2.

Raymond, J., Langevin, H., Comeau, F.A., Malo, M., 2022. Temperature dependence of rock salt thermal conductivity: Implications for geothermal exploration. Renew. Energy 184, 26–35. https://doi.org/10.1016/J.RENENE.2021.11.080.

Reyer, D., 2013. Outcrop Analogue Studies of Rocks from the Northwest German Basin for Geothermal Exploration and Exploitation: Fault Zone Structure, Heterogeneous Rock Properties, and Application to Reservoir Conditions.

Richard, J., Sizun, J.P., 2011. Pressure solution-fracturing interactions in weakly cohesive carbonate sediments and rocks: example of the synsedimentary deformation of the Campanian chalk from the Mons Basin (Belgium). J. Struct. Geol. 33, 154–168. https://doi.org/10.1016/J.JSG.2010.11.006.

Riepe, L., Sachs, W., Schopper, J.R., 1983. Pressure effect on permeability. In: Trans. 8th European. Format. Evaluat. Symp. Of the SPWLA. London, pp. 1–24.

Robion, P., David, C., Dautriat, J., Colombier, J.C., Zinsmeister, L., Collin, P.Y., 2014. Pore fabric geometry inferred from magnetic and acoustic anisotropies in rocks with various mineralogy, permeability and porosity. Tectonophysics 629, 109–122. https://doi.org/10.1016/j.tecto.2014.03.029.

Roure, F., Choukroune, P., Berastegui, X., Munoz, J.A., Villien, A., Matheron, P., Bareyt, M., Seguret, M., Camara, P., Deramond, J., 1989. Ecors deep seismic data and balanced cross sections: Geometric constraints on the evolution of the Pyrenees. Tectonics 8, 41–50. https://doi.org/10.1029/TC008I001P00041.

Sass, I., Götz, A.E., 2010. Thermofacies: key to geothermal reservoir characterization. EGU General Assembly 12, 2892.

Sass, I., Götz, A.E., 2012. Geothermal reservoir characterization: a thermofacies concept. Terra Nova 24, 142–147. https://doi.org/10.1111/j.1365-3121.2011.01048.x.

Sass, J.H., Stone, C., Munroe, R.J., 1984. Thermal Conductivity determinations on Solid Rock, a Comparison between a Steady-State Divided-Bar and a Commercial Transcient Line-Source device. J. Volcanol. Geotherm. Res. 20, 145–153.

Sass, I., Weydt, L., Götz, A.E., Machel, H.G., Heldmann, C.-D.J., 2020. Geothermal Reservoir Analogues on a Continental Scale: Western Canadian Sedimentary Basin versus Northern Alpine Molasse Basin. In: PROCEEDINGS World Geothermal Congress 2020+1, pp. 1–9.

Saura, E., Oró, Ardèvol I., Teixell, A., Vergés, J., 2016. Rising and falling diapirs, shifting depocenters, and flap overturning in the Cretaceous Sopeira and Sant Gervàs subbasins (Ribagorça Basin, southern Pyrenees). Tectonics 35, 638–662. https://doi.org/10.1002/2015TC004001.

Scheck-Wenderoth, M., Cacace, M., Maystrenko, Y.P., Cherubini, Y., Noack, V., Kaiser, B. O., Sippel, J., Björn, L., 2014. Models of heat transport in the central European Basin System: Effective mechanisms at different scales. Mar. Pet. Geol. 55, 315–331. https://doi.org/10.1016/J.MARPETGEO.2014.03.009.

Schön, J., 2015. Physical Properties of Rocks: Fundamentals and Principles of Petrophysics, 2nd ed. Elsevier.

Serra-Kiel, J., Mató, E., Saula, E., Travé, A., Ferràndez-Canadell, C., Busquets, P., Samsó, J.M., Tosquella, J., Barnolas, A., Àlvarez-Pérez, G., Franquès, J., Romero, J., 2003a. An inventory of the marine and transitional Middle/Upper Eocene deposits of the Southeastern Pyrenean Foreland Basin (NE Spain). Geol. Acta 1, 201–229.

Serra-Kiel, J., Travé, A., Mató, E., Saula, E., Ferràndez-Cañadell, C., Busquets, P., Tosquella, J., Vergés, J., 2003b. Marine and Transitional Middle/Upper Eocene units of the Southeastern Pyrenean Forelan Basin (NE spain). Geol. Acta 1, 177–200.

Sun, X., Alcalde, J., Gomez-Rivas, E., Owen, A., Griera, A., Martín-Martín, J.D., Cruset, D., Travé, A., 2021a. Fluvial sedimentation and its reservoir potential at foreland basin margins: a case study of the Puig-reig anticline (South-eastern Pyrenees). Sediment. Geol. 424, 105993 https://doi.org/10.1016/J.SEDGEO.2021.105993.

Sun, X., Gomez-Rivas, E., Alcalde, J., Martín-Martín, J.D., Ma, C., Muñoz-López, D., Cruset, D., Cantarero, I., Griera, A., Travé, A., 2021b. Fracture distribution in a folded fluvial succession: the Puig-reig anticline (South-Eastern Pyrenees). Mar. Pet. Geol. 132, 105169 https://doi.org/10.1016/J.MARPETGEO.2021.105169.

Sun, X., Gomez-Rivas, E., Cruset, D., Alcalde, J., Muñoz-López, D., Cantarero, I., Martín-Martín, J.D., John, C.M., Travé, A., 2022. Origin and distribution of calcite cements in a folded fluvial succession: the Puig-reig anticline (South-Eastern Pyrenees). Sedimentology. https://doi.org/10.1111/sed.12994.

Sussman, A., 2002. Thrust belt curvature: Structural and paleomagnetic analyses in the Catalunyan Pyrenees and Sevier orogen. PhD Thesis.

Sussman, A., Curtin, T.M., 2002. Structural and stratigraphic controls on the development of joints within the Oliana Anticline, southern Pyrenees, Spain. Geol. Soc. Am. Ab. Prog. 34, 165.

Sussman, A., Butler, R.F., Dinarès-Turell, J., Vergés, J., 2004. Vertical-axis rotation of a foreland fold and implications for orogenic curvature: an example from the Southern Pyrenees, Spain. Earth Planet. Sci. Lett. 218, 435–449. https://doi.org/10.1016/S0012-821X(03)00644-7.

Teixell, A., Labaume, P., Ayarza, P., Espurt, N., de Saint Blanquat, M., Lagabrielle, Y., 2018. Crustal structure and evolution of the Pyrenean-Cantabrian belt: a review and new interpretations from recent concepts and data. Tectonophysics 724–725, 146–170. https://doi.org/10.1016/J.TECTO.2018.01.009.

Tester, J.W., Drake, E.M., Driscoll, M.J., Golay, M.W., Peters, W.A., 2012. Sustainable Energy, Choosing among Options, second ed. MIT Press.

Travé, A., Serra-Kiel, J., Zamarreño, I., 1996. Paleoecological interpretation of transitional environments in Eocene carbonates (NE Spain). Palaios 11, 141–160. https://doi.org/10.2307/3515067.

Vasseur, G., Brigaud, F., Demongodin, L., 1995. Thermal conductivity estimation in sedimentary basins. Tectonophysics 244, 167–174. https://doi.org/10.1016/0040-1951(94)00225-X.

Vergés, J., 1993. Estudi tectònic de la vessant sud del Pirineu central i oriental. Evolució cinemàtica en 3D. PhD Thesis.

Vergés, J., Muñoz, J.A., 1990. Thrust sequences in the southern central Pyrenees. Bulletin de la Société Géologique de France 4, 265–271. https://doi.org/10.2113/gssgfbull.VI.2.265.

Vergés, J., Muñoz, J.A., Martínez, A., 1992. South Pyrenean fold and thrust belt: The role of foreland evaporitic levels in thrust geometry. In: MCClay, K.R. (Ed.), Thrust Tectonics. Springer, Dordrecht, pp. 255–264. https://doi.org/10.1007/978-94-011-3066-0_23.

Vergés, J., Fernàndez, M., Martínez, A., 2002. The Pyrenean orogen: Pre-, syn-, and post-collisional evolution. In: Rosebaum, G., Lister, G.S. (Eds.), Reconstruction of the Evolution of the Alpine-Himalayan Orogen. Journal of the Virtual Explorer, pp. 55–74. https://doi.org/10.3809/jvirtex.2002.00058.

Vernoux, J.F., Genter, A., Razin, P., Vinchon, C., 1995. Geological and Petrophysical Parameters of a Deep Fractured Sandstone Formation as Applied to Geothermal Exploitation EPS-1 Borehole, Soultz-Sous-Forets. BRGM (Report), France.

Vidal, J., Genter, A., Chopin, F., Dalmais, E., 2016. Natural fractures and permeability at the geothermal site Rittershoffen, France. In: European Geothermal Congress, pp. 1–8.

Watkins, H., Healy, D., Bond, C.E., Butler, R.W.H., 2018. Implications of heterogeneous fracture distribution on reservoir quality; an analogue from the Torridon Group sandstone, Moine Thrust Belt, NW Scotland. J. Struct. Geol. 108, 180–197. https://doi.org/10.1016/j.jsg.2017.06.002.

Worden, R.H., Mayall, M.J., Evans, I.J., 1997. Predicting reservoir quality during exploration: lithic grains, porosity and permeability in Tertiary clastic rocks of the South China Sea basin. Geol. Soc. Lond., Spec. Publ. 126, 107–115. https://doi.org/10.1144/GSL.SP.1997.126.01.08.

Yang, Y., Aplin, A.C., 2010. A permeability-porosity relationship for mudstones. Mar. Pet. Geol. 27, 1692–1697. https://doi.org/10.1016/j.marpetgeo.2009.07.001.

Zinszner, B., Pellerin, F.M., 2007. A geoscientist's Guide to Petrophysics, Technip. ed. A Geoscientist's Guide to Petrophysics. Editions Technip, Paris.